

## Dimensionless morphological ratios versus stream power variations at bankfull stage in an ephemeral channel

Carmelo Conesa-García <sup>a,\*</sup>, Pedro Pérez-Cutillas <sup>a</sup>, Rafael García-Lorenzo <sup>a</sup>, Joris Eekhout <sup>b</sup>, Álvaro Gómez-Gutiérrez <sup>c</sup>, Agustín Millares-Valenzuela <sup>d</sup>, Alberto Martínez-Salvador <sup>a</sup>

<sup>a</sup> University of Murcia, Department of Geography, Murcia, Spain

<sup>b</sup> Centre for Applied Soil Science and Biology of the Segura (CEBAS) (CSIC), Soil and Water Conservation Research Group, Murcia, Spain

<sup>c</sup> University of Extremadura, GeoEnvironmental Research Group, Cáceres, Spain

<sup>d</sup> Group of Environmental Fluid Dynamics, Andalusian Institute for Earth System Research (IISTA), University of Granada, Granada, Spain



### ARTICLE INFO

#### Article history:

Received 30 January 2020

Received in revised form 3 April 2020

Accepted 4 April 2020

Available online 08 April 2020

#### Keywords:

Dimensionless morphological ratios

Stream power

Bankfull stage

Spatial patterns

Ephemeral streams

### ABSTRACT

Dimensionless morphological ratios (DMR) generally are used in systemic proposals for stream classification and river restoration projects. Often, such morphometric parameters, including field data from channel cross sections, develop into a template for a given geomorphic reference site. In this study, high-resolution Digital Terrain Models (HRDTMs), combined with orthophotos from 2018 and ground-based surveys, were used to analyze the spatial variability of DMR in a semi-arid ephemeral stream subject to changes in stream power under bankfull conditions. In particular, a channel reach of 2.7 km in length along the Upper Mula stream in southeastern Spain was chosen to test the relationships between the two types of variables. Rosgen's DMR (width to depth ratio, entrenchment ratio, bank height ratio) and hydraulic data at bankfull stage (flow velocity, Froude number, shear stress, mean stream power and energy gradient, among others) were calculated by 1D hydrodynamic modeling and HRDTMs prior entry of field information. The resulting maps allowed comparison of stream power with DMR in relation to the channel stretch class and bed stability. The results showed similar spatial patterns for the width to depth ratio and the bank height ratio. The average values estimated in bend stretches were lower than along straight and slightly sinuous stretches and very similar to those of sub-reaches from the inflection point to the meander bend apex. However, the entrenchment ratio followed a different pattern, according to which the straight and slightly sinuous stretches were the most entrenched and the bend stretches presented a more moderate average entrenchment ratio. In addition, the energy balance and power gradient also experienced spatial variations in relation to the bed stability and DMR. Only in highly incised sub-reaches were such relationships not significant. The lack of a significant correlation between excess energy and bank height ratio or width to depth ratio over short lag distances was also verified, regardless of the affected bedforms. An ANOVA showed important differences between the straight and slightly sinuous stretches and bend stretches, which were strongly influenced by the incision and entrenchment ratios and the maximum bankfull depth.

© 2020 Elsevier B.V. All rights reserved.

## 1. Introduction

Ephemeral streams are watercourses of arid and semi-arid environments with unstable morphology and high temporal variability of runoff. Sudden, extreme discharge events that are isolated in time, alternate with long dry periods. These types of streams are particularly sensitive to short-term climatic changes, and human impacts may alter their degree of response, sometimes leading to large morphological adjustments during flash floods

(Bull, 1997; Segura-Beltrán and Sanchís-Ibor, 2013; Norman et al., 2017). As a result, the ephemeral channels show a changing geometry, highly conditioned by differences in slope and textural variations in the bed materials and banks. Often along their upper reaches and on alluvial fans, these channels have a steep slope that promotes a fast hydraulic regime. Under such conditions, and considering the abundant sediment stored within the channel, important transport rates contribute to most of the morphological changes in the channel. The streambed is usually very permeable, so flood peak discharges can decrease sharply downstream because of transmission losses (Goodrich et al., 1997; Shaw and Cooper, 2008). In addition, the sediment transport capacity decreases while the bed degradation and storage of subsoil moisture increases (Merritt and Wohl, 2003; Camporeale et al., 2006; Reid and Frostick, 2011). This explains why the longitudinal channel profile is not concave

\* Corresponding author.

E-mail addresses: [cconesa@um.es](mailto:cconesa@um.es) (C. Conesa-García), [jekhout@cebas.csic.es](mailto:jekhout@cebas.csic.es) (J. Eekhout), [alvg0@unex.es](mailto:alvg0@unex.es) (Á. Gómez-Gutiérrez), [\(A. Millares-Valenzuela\).](mailto:mivalag@ugr.es)

like that of a perennial river, but is rather straight, with a constant bed slope (Martín-Vide, 1997; Chen et al., 2019). The rapid rise and fall of the flood discharges makes bed behavior unpredictable, and high erosion rates (transitory or permanent) and sedimentary accretion can occur.

The dimensions and shape of ephemeral streams in semi-arid environments are mainly controlled by changes in slope, hydraulic roughness and transport efficiency. According to the stream channel pattern such changes may reflect systematic adjustments of stream power ( $\omega$ )/resisting power ( $\omega_c$ ) ratios ( $\omega/\omega_c$ ) (Bull, 1997), which also affect the channel geometry (Biron et al., 2013; Bazzi and Lerner, 2015). Geomorphic dimensions and dimensionless ratios have been used in different stream classifications (Rosgen, 1997; Brierley and Fryirs, 2005; Kasprak et al., 2016) and as indicators of physical variability for natural channel restoration plans (Wampler, 2012; Ezzat and Oak, 2012). Normally templates of dimensionless ratios from geomorphic reference sites are used to compare different stream stretches, regarding their cross sections and planforms.

Morphologic relationships for channel variability are described and quantitatively related to the driving forces of different ephemeral channel stretches. These streams frequently present diverse entrenchment ratios along the reach. Here, the current bankfull channel does not always turn out to be significantly wider at bendways than in inter-bend straight stretches. In fact, it is characterized by a variable geometry and can be quite different from how it was in the past. Channel migration rates are likely to be low unless the banks are stabilized and the point bars are well-developed only in the tightest bends.

Until now, scarce attention has been paid to the spatial variability of changes in geometry for ephemeral streams in semi-arid environments, as a function of channel pattern and variations in stream power (Levick et al., 2008; Ortega et al., 2014). In this respect, the study site, located in the Upper Mula stream, a tributary of the Segura River, provides a good example for the analysis of such relationships within the context of Mediterranean semi-arid conditions characterized by rapid runoff responses and related driving forces.

We started this work with a previous lack of knowledge about the geomorphic reference sites in the stream reach under study, deducing it later from the cross sections that reflect a minimum expenditure of energy and an equal distribution of stream power. Instead of templates, the spatial interpolation of geometric parameters and dimensionless ratios obtained from channel cross sections extracted from high-resolution Digital Terrain Models (HRDTM) is proposed here.

Two primary objectives were considered: (1) to evaluate the spatial distribution of adjustments in channel geometry for the study reach and the different stretch classes, according to the sinuosity and curvature degree, and (2) to determine if the observed changes could be statistically related to the flow energy variations of the Upper Mula stream. For the first objective, dimensionless morphological ratios (DMR) were mapped and spatially related to each other along the whole reach and according to their location in different stretch classes (bendways and inter-bend straight stretches). In this regard, it is worth checking the pattern described by each relationship. A high positive correlation between the entrenchment ratio (ER) and the incision ratio (IR), for example, will mean that the most entrenched cross sections have the lowest incision values, and vice versa.

The second objective was tested by examining different hypotheses:

(1) The  $\omega$  thresholds usually related to morphological adjustments in perennial, gravel-bed streams may be different from those required in ephemeral channels with variable bed stability and IR range.

(2) Variations in  $\omega$  values affect bed stability to different degrees depending on the stretch planform and sinuosity.

(3) Patterns of the mean stream power gradient ( $\partial\omega/\partial s$ ),  $\omega/\omega_c$  and the bedform stability index (BFS) can be found from their relationships with different ranges of the DMR. For example, stretches with a greater change in channel cross sections could coincide with larger positive and negative values of  $\partial\omega/\partial s$ .

(4) Locations with the greatest  $\omega/\omega_c$  ratios will have the greatest bed scouring, but this does not necessarily imply an increase in IR. This ratio depends more on the lowest bank height and the maximum bankfull depth. Instead, locations where  $\omega$  surpasses  $\omega_c$  will have the lowest excess energy per unit bed area ( $\epsilon$ ) and the most stable bedforms.

(5) At similar ranges of  $\epsilon$ , the width to depth ratio (WDR) along bends with pools and point bars are lower than in stretches with riffles and steps. Such a pattern is not expected for the relationships between IR and  $\epsilon$ .

(6) The  $\epsilon$  values calculated for a given cross section will lose their effect on the IR and the WDR, according to the distance downstream from that cross section, regardless of the goodness of fit between such variables.

## 2. Study area and environmental conditions

The study site is located in the lower part of the Upper Mula stream, a tributary of the Segura River on its right bank (Fig. 1). This is an ephemeral stream draining the Upper Mula watershed (169 km<sup>2</sup>) to the La Cierva reservoir. The relief shows a range of elevations, varying from 1392 m in headwater areas to 232 m in lower areas. The whole basin is framed within the Subbetic Domain (Betic Cordillera, southeastern Spain), where Alpine orogeny and subsequent tectonic activity deformed the previous structures and created seismic foci, subvolcanic rock outcrops and strike-slip faults (Rodríguez Estrella and Navarro Hervás, 2001). Limestones, dolomites and limestone marls of Jurassic age mainly appear in the headwater areas, while Quaternary alluvial sediment and Miocene marls predominate in the middle and lower basin, respectively.

The predominance of soft materials (marls, silts and clays), together with semi-arid climatic conditions, low average annual rainfall (329 mm in the La Cierva reservoir and around 370 mm in the header area), an irregular pluviometric regime and torrential rains, and a sparse vegetation cover, make this basin a territory especially vulnerable to soil erosion. The greatest losses of soil and sediment loads are produced when heavy downpours occur. Under such conditions, the Upper Mula stream and its main tributaries experience large flash floods with an abundant solid load. In addition, recent changes in land use have favored channel incision. The area of forest (shrub and tree areas) in the headwater mountains decreased ≈3.6% between 1956 and 2016, while its density increased because of the abandonment of traditional silviculture and forestry as well as the implementation of reforestation from 1955 to 1971 (Martínez Salvador et al., 2015). The headwater area was also part of a hydrological correction project (2001–2003) that involved the building of six check dams of gabions and masonry and 600 m<sup>3</sup> of *albarradas* (CHS, 2002). A dozen check dams already existed in the basin, at least since the early 1980s, as seen in orthophotographs.

The studied channel reach has a length of 2.7 km and an average slope of 0.76%. The Upper Mula stream has a mixed planform, including meandering and straight to sinuous stretches, with a variety of both channel geometries and bank materials. It is a gravel-bed stream typically characterized by riffles and pools in bends and runs in straight to sinuous stretches. A dominant downcutting in the past has locally exhumed the rocky substrate and old large blocks, especially in the less sinuous channel reaches (Fig. 2). This channel is generally characterized by intermediate width-to-depth ratios, moderate to high entrenchment and significant incision rates. The grain size of bed materials is variable and mainly depends on the location in active or stable bedforms: medium-grained bed material (sand and gravel) predominates in the inter-bend runs, medium and coarse gravels in highly stable point bars, and fine sediments (clay and silts) in bend pools. The banks also offer different resistance to erosion as they are composed of alluvial material, marls or loamy limestones.

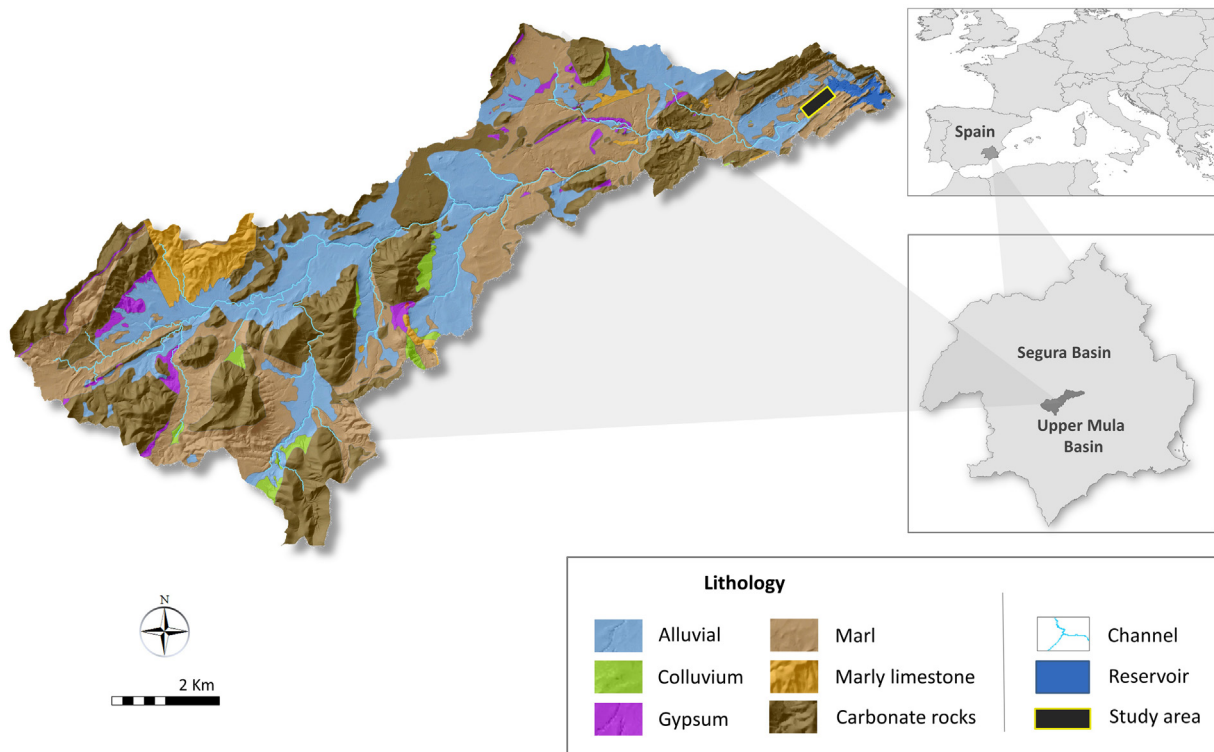


**Fig. 1.** Location of the study area (Upper Mula catchment) in the Segura basin, Southeastern Spain. Map depicting the drainage network and the spatial distribution of rock types.

### 3. Materials and methods

The bankfull stage along each reach was determined from field indicators (see Section 3.3) and the HRDTM developed from UAV and Global Navigation Satellite System (GNSS) data. All the data were then transferred to the 1D hydrodynamic model HEC-RAS ([USACE \(United States Army Corps of Engineers\)](#), 2002) to get the channel profile and cross sections (separated from each other by 5 m) and their corresponding hydraulic parameters. Using a GIS to integrate the HRDTM, field measurements and hydraulic geometry data, DMR were calculated and mapped for the channel reaches.

#### 3.1. SfM-MVS photogrammetry

The study area was surveyed using a fixed-wing UAV (Ebee model by Sensefly) with a Sony WX220 Sensor (18 Mpx) to acquire 728 high-resolution aerial images. The flight track and parameters were pre-programmed using the eMotion 3 software. Three flights were carried out to cover the geographic extent of the study area: two to cover the area with perpendicular flight lines and one using the corridor option following the axis of the channel. In order to get cm-level accuracies, 11 artificial GCPs were marked in the field and measured by means of two (base and rover) GNSS receivers in Post Processing Kinematic mode (using GPS + GLONASS solutions).

After each flight eMotion 3 software was used to download the images and the coordinates of the UAV path. This information was used as input in Pix4Dmapper Pro software (v.3.1.18) together with the GCPs coordinates to produce the point cloud (Fig. 3), the HRDTM and high-resolution orthophotographs of the study reach (Fig. 4).

The processing of the dataset followed the classical Structure-from-Motion and MultiView Stereo photogrammetry workflow (e.g., [Tammenga et al., 2015](#), [Alfonso-Torreño et al., 2019](#); [Hamshaw et al., 2019](#)). GCPs were used to georeference the 3D models and improve the camera calibration before the bundle adjustment. A Ground Sampling Distance of 3.0 cm and a Root Mean Square Error of 2.8 were

achieved. The resulting 3D point cloud comprised 335 million points with an average point density of 366 points  $\text{m}^{-2}$ .

#### 3.2. Channel centerline analysis

The channel reach was subdivided into two categories: (1) bend stretches (BS) and straight stretches (SS) and (2) stretches from the inflection point to the meander bend apex (IP-MBA) and stretches from the meander bend apex to the inflection point (MBA-IP). We first obtained the channel centerline from the bankfull bank lines through the method described by [Golly and Turowski \(2017\)](#). Then the curvature was determined with the following equation:

$$C = \frac{\alpha_y \beta_x - \alpha_x \beta_y}{k^3} \quad (1)$$

where  $\alpha_x = \text{coord}_x(j) - \text{coord}_x(j-k)$ ;  $\alpha_y = \text{coord}_y(j) - \text{coord}_y(j-k)$ ;  $\beta_x = \text{coord}_x(j+k) - \text{coord}_x(j)$ ;  $\beta_y = \text{coord}_y(j+k) - \text{coord}_y(j)$ ; and  $k = 80 \text{ m}$ .

From the curvature series, the inflection points were obtained where the curvature crosses 0 (Fig. 5). The meander bend apices were obtained at the local optima (positive or negative) between two inflection points. Next, a sinuosity threshold of 1.2 was used to differentiate between BS and SS, where a value of the sinuosity series higher than the threshold signifies a bend section and a value lower than the threshold signifies a straight channel reach. The subdivision was subsequently used to determine the average of the indices per stretch. The length and delimitation of both planform types coincided with those of [Mueller's \(1968\)](#) sinuosity index (SI):  $SI < 1.05$  for SS and  $SI > 1.05$  for reaches with BS, including two classes: sinuous ( $1.05 < SI < 1.5$ ) and meandering ( $SI > 1.5$ ).

#### 3.3. Measures of the channel and dimensionless morphological ratios (DMR)

The bankfull channel dimensions (bankfull width, maximum and mean bankfull depth) were surveyed in the field for 27 cross sections,



**Fig. 2.** Pool next to the bend apex in an entrenched channel reach (a and b); riffles and exhumed blocks in straight stretches with local rocky bed outcrops (c); erodible banks composed of alluvial materials (d and e); vegetated gravel bars at the entrance of a sharp meander bend (f).

equidistant (around 100 m) from each other. They were then implemented in GIS using a HRDTM and the output from the HEC-RAS to obtain, by spatial interpolation, these physical parameters for 266 cross sections with a 5 m interval along the study reach (Conesa-García et al., 2019). Bankfull stage was identified using field indicators such as significant breaks in bank slope, changes in vegetation, top of the bank, marks of erosive flows and back of point bars (Leopold, 1994; Wharton, 1995; Rosgen, 1996). Other Rosgen physical parameters of

streams, such as flood prone width, bank height, streambed slope and sinuosity, and DMR (WDR, ER and IR) were also calculated using GIS from the same HRDTM and mapped for the whole reach.

### 3.3.1. Width-to-depth ratio (WDR)

The WDR was calculated by dividing the bankfull width by the mean bankfull depth. As is widely reported in the literature, the width and depth reflect flow magnitudes and sediment load over time (Zones,



**Fig. 3.** Detail of the resulting 3D point cloud for a meandering stretch in the stream reach studied.

2004), so that their relationship at bankfull stage can be used to express the flow-competence and transport capacity during discharges responsible for the current active channel form. It is an indicator of the channel shape that is independent of stream size and helps us to understand the distribution of available energy within the channel (Rosgen, 1996; Stewardson, 2005). In other studies, the WDR has also been considered a function of the dominant sediment texture on the channel perimeter (Schumm, 1960; Richards, 1982) and the boundary conditions (geological constraints, valley slope, channel substrate and riparian vegetation) that control the form of a channel reach (Charlton, 2008). Under such conditions, the WDR is adjusted by the erosion-sedimentation balance within the channel, causing bed accretion or degradation and displacement of banks (Simon and Castro, 2003).

In addition, two dimensionless parameters were used to describe the variability of the bankfull channel width around meander bends: (1) the bend apex width to inflection point width ratio ( $W_a/W_i$ ), and (2) the ratio of the width at the location of maximum bend pool scour to the inflection point width ( $W_p/W_i$ ). Theoretically, the values of these parameters change according to the degree of curvature and the type of meander bend. Following the criteria of the NRCS (2007a), both ratios were related to the SI, which was used as the independent variable, rather than the radius of curvature-to-width ratio.

### 3.3.2. Entrenchment ratio (ER)

This ratio was estimated as the flood prone width divided by the bankfull width. In relative terms, the ER reflects the vertical containment of a channel and the capacity of its floodplain to laminate overbank discharges. Three categories of entrenchment, based on criteria of Rosgen (1996), were adopted: high (ER < 1.4), moderate (ER = 1.4–2.2) and low (ER > 2.2). According to Rosgen (1997), during floods highly entrenched reaches can contain all the flow within the channel itself and it does not spill out onto the floodplain. In moderately entrenched stretches, high water levels can cover much of the flood prone area while stream segments showing little or no entrenchment connect their floodplain directly to bankfull flows. This ratio provides appropriate information about channel morphology, in contrast to

hydrological entrenchment ratios, like the Walters et al. (2003) entrenchment ratio, and the relative discharge ratio (Luebke, 2006), both based on the average overbank discharge. The ER values may be associated with many factors, including variations in climate, local tectonic lowering of the base level and human impacts (Bull, 1997). The most immediate cause is an increase in the erosiveness of stream flows for materials of low erosional resistance.

### 3.3.3. Incision ratio (IR)

The bank height ratio (BHR) (Rosgen, 1996) was adopted as the IR, calculated by dividing the lowest bank height (LBH) by the maximum bankfull depth (MD<sub>bf</sub>). Incision ratios are valuable because they are a more sensitive measurement of bed degradation than the entrenchment ratio, allowing one to identify the occurrence of a degradation process in its most recent stage. Where the floodplain is wider in relation to the bankfull width, a larger incision and formative-discharge is required to produce significant changes in the ER. Any change in the ER usually involves more substantial changes in the IR and will be subject to flood peaks with longer return times ( $\geq 50$ -yr floods). Incision ratios close to one indicate bed stability during the last phases of channel formation. In contrast, incision ratios  $> 1$  reflect recent downcutting or bed degradation processes, which may be relevant ( $1.5 < IR < 2$ ) or very intense ( $IR > 2$ ). Along the study reach two lowest bank heights were observed, resulting in an upper and lower IR. The IR and the ER were also used together to quantify floodplain connectivity.

### 3.4. Bed stability indicators

Two substrate stability indicators were adopted: (1) the “Relative Bed Stability” (RBS) index and (2) the “Bedform Stability” (BFS) index. The RBS index, described by Olsen et al. (1997), defines bed stability as the ratio between the critical shear stress required to mobilize the D<sub>84</sub> size particle ( $\tau_{c84}$ ) and the shear stress at bankfull flow ( $\tau_{bf}$ ). The critical bed shear stress is calculated using the form of the Shields

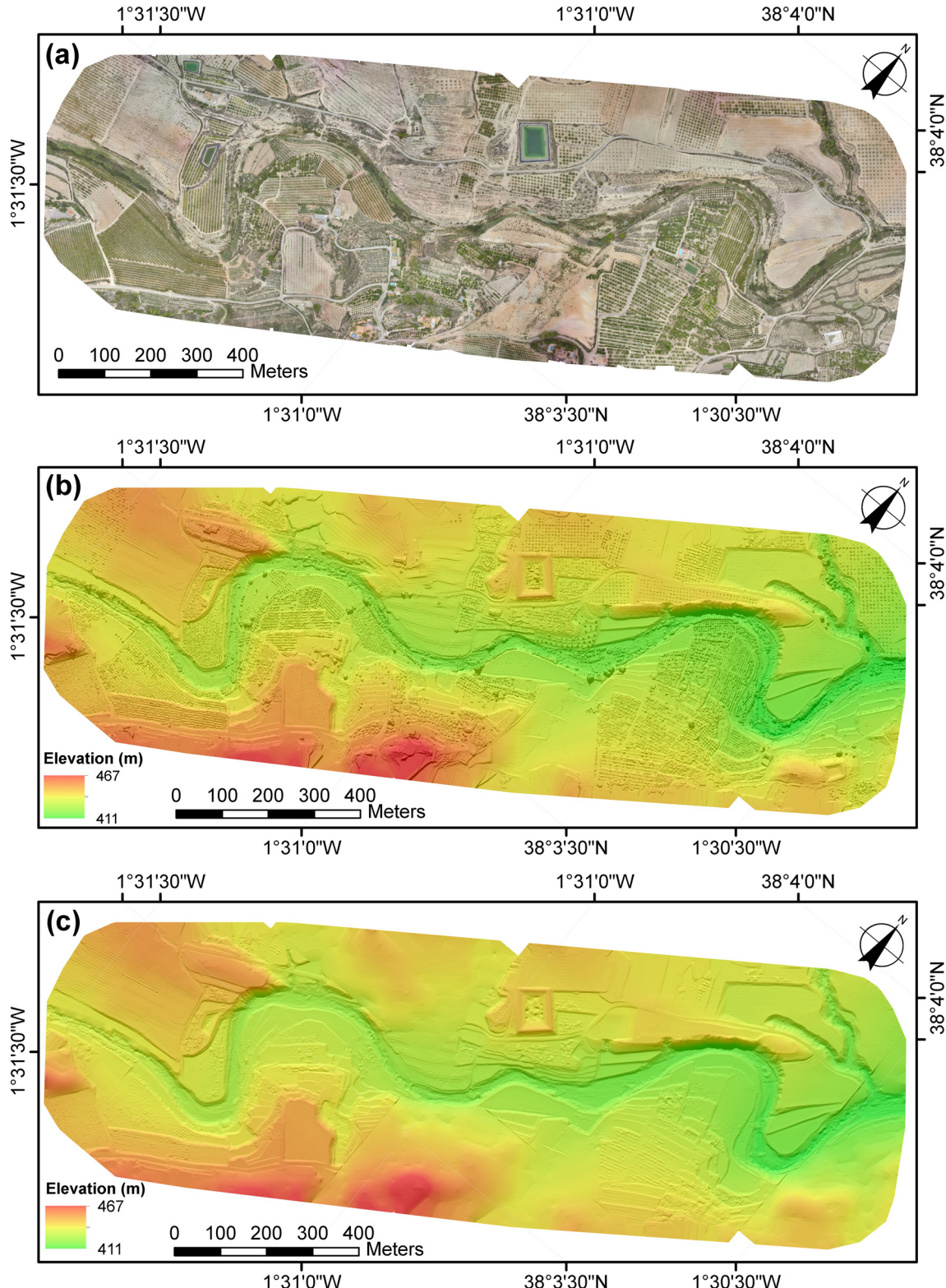


**Fig. 4.** Cartographic products obtained from the UAV and SfM-MVS photogrammetric workflow: (a) orthophoto (3 cm pixel size), (b) Digital Surface Model (3 cm pixel size) and (c) Digital Elevation Model (15 cm pixel size).

equation in Olsen et al. (1997):

$$\tau_{c84} = \tau_c^*(\rho_s - \rho)gD_{84} \quad (2)$$

where  $\rho_s$  and  $\rho$  represent the sediment and water densities, respectively,  $g$  is the acceleration due to gravity and  $\tau_c^*$  are is the critical

value of the dimensionless Shields parameter. The shear stress at bankfull flow is determined as:

$$\tau_{bf} = \rho g R S \quad (3)$$

where  $R$  is the hydraulic radius and  $S$  is the water surface slope. The

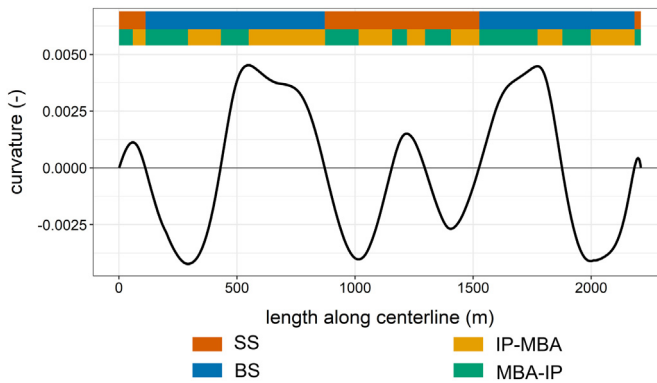


**Fig. 5.** Length and delimitation of each channel stretch class according to the degree of curvature and the sinuosity index. The channel centerline was obtained from the bankfull limit-lines.

relative bed stability index is then defined as:

$$\tau_{bf} = \tau_{c84}/\tau_{bf} \quad (4)$$

If  $\tau_{bf}$  is  $>1$ , the bed is presumed to be fully mobilized only for events larger than bankfull and the channel is relatively stable. Conversely, if  $\tau_{bf}$  is  $<1$ , the bed is mobilized at sub-bankfull flows and the channel is presumed to be unstable.

The BFS index, proposed here, can be considered an index of the relative stability of the bedforms; for bankfull conditions ( $BFS_{bf}$ ), it was

determined from the following expression:

$$BFS_{bf(i)} = \left[ \left( \sum v_{rgu(i)} \cdot w_{rgu(i)} \right) / W_{bf(i)} \right] / n_{rgu(i)} \quad (5)$$

where  $v_{rgu}$  is the value assigned to each type of bed geomorphic unit (bgu), depending on its resistance to erosion observed in recent bankfull flows,  $w_{rgu}$  is the width of each bgu in a given channel cross section,  $W_{bf}$  is the bankfull width, and  $n_{rgu}$  is the number of bgu. In our case  $n_{rgu} = 7$ : (1) active channels, secondary minor channels/runs and pools; (2) low active bars; (3) high active bars; (4) bank-failure deposits and deposits from external sources; (5) scant vegetated bars; (6) vegetated bars; (7) exhumed rocky beds and old sediment areas. Such classes were extracted from the map of the bgu identified within the boundaries of the bankfull channel (Fig. 6). This index varies between 0 and 1, and the value of 0.5 is a threshold that discriminates in relative terms between stable and unstable bedforms.

In addition, the locational weight of each bgu, based on its relative presence in different stretch classes was calculated as

$$LW_{rgu(sc)} = \sum (w_{rgu(i)} / W_{bk(i)}) / n_{i(sc)} \quad (6)$$

where  $LW_{rgu(sc)}$  is the locational weight assigned to each bgu depending on the surface area it occupies with respect to the total area of a given stream stretch class (sc),  $w_{rgu}$  is the width of a bgu for each cross section (i),  $W_{bk}$  is the total bed width under bankfull conditions for i, and  $n_{i(sc)}$  is the number of cross sections included in each stretch class.

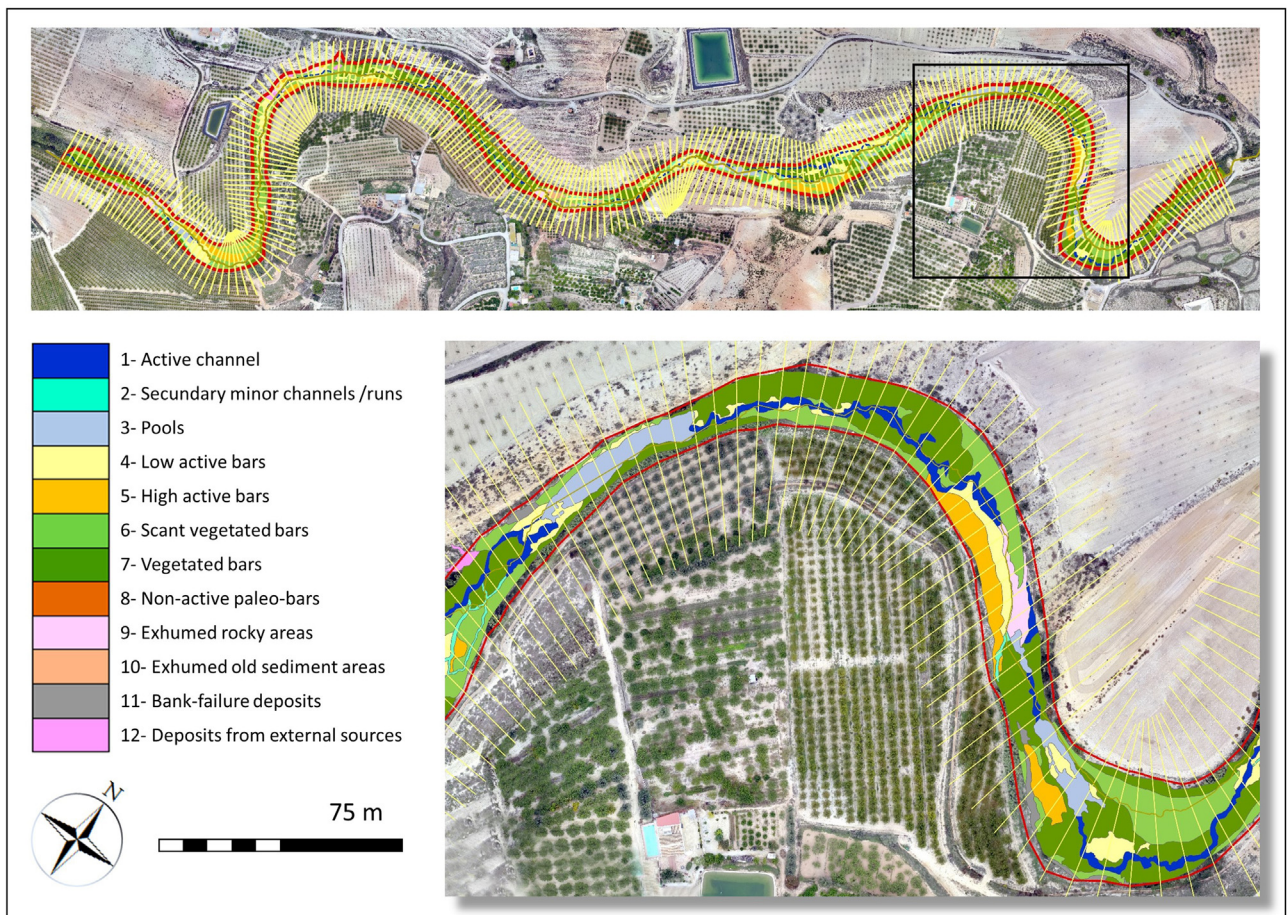


**Fig. 6.** Raster layer showing bedforms within the bankfull limits and the overlay of vector segments displaying cross sections for which  $BFS_{bf}$  and  $LW_{rgu}$  were calculated.

### 3.5. Mapping stream power variations at bankfull stage

In addition to channel geometry, the HRDTM implemented using HEC-RAS also allowed us to obtain estimations of velocities, roughness, and water discharges from the 27 sections monitored. Based on the cross sections an average bankfull stage was considered under subcritical flow conditions. This bankfull threshold was then applied to 266 cross sections obtained by interpolation, maintaining between them a distance of 10 m in straight channel reaches and 5 m in bends. For each section, information was obtained about the flow surface, hydraulic radius, velocity, shear stress and bankfull channel geometry. The power per unit length of stream ( $\Omega$ ) and mean stream power ( $\omega$ ) at bankfull discharge ( $Q_{bf}$ ) were calculated for all cross sections (Leopold et al., 1964):

$$\Omega = \gamma Q S_w \quad (7)$$

$$\omega = \Omega / w \quad (8)$$

where  $\gamma$  is the specific weight of water ( $N\ m^{-3}$ ),  $Q$  is the discharge ( $m^3/s$ ),  $S_w$  is the water surface slope ( $m/m$ ), which is used to estimate the energy gradient, and  $w$  is the water-surface width (m).  $\Omega$  represents the energy dissipation per unit channel length and  $\omega$  the energy expenditure per unit bed area. The width, average depth and maximum bankfull depth for each cross section and its corresponding raster cell were acquired from the bankfull channel polygons. The mean stream power gradient ( $\partial\omega/\partial s$ ) was calculated by subtracting  $\omega$  in cross-sectional cell  $i$  from  $\omega$  in cell  $i - 1$  and dividing the result by the distance between the centroid of each pair of consecutive cells along the channel centerline. In this way positive  $\partial\omega/\partial s$  values indicate downstream increases in  $\omega$ , while a negative value indicates that  $\omega$  decreases from one cell to the next (Lea and Legleiter, 2015). Parentheses are used here after to denote the location (e.g.,  $\omega$  at cell  $i$  would be denoted as  $\omega(i)$ ).

The energy expenditure beyond the critical mean stream power ( $\omega_c$ ) in each cross-sectional cell was estimated in addition to  $\partial\omega/\partial s$  to understand the spatial distribution of the energy available for sediment transport and morphological channel adjustments during bankfull discharges. The excess energy per unit bed area ( $\varepsilon$ ) expended over  $\omega_c$  at this stage was determined by calculating  $\omega$  from the mean bankfull discharge ( $Q_{bf}$ ) and comparing the values to the  $\omega_c$  obtained using Eqs. (10) and (16) from Parker et al. (2011), which relate  $\omega_c$  to slope and grain size. The bed slope was extracted from the HRDTM described above. A representative reach pebble count was made along transect stretches from one stream bank to the other in bankfull sections with similar bed features, while riffle cross sections were sampled using the active bed riffle pebble count. The median grain size ( $D_{50}$ ) and 84th percentile ( $D_{84}$ ) were calculated for each transect, extending their values to the set of cross sections included in it. In addition, the energy balance was estimated as the ratio resulting from the division of  $\omega$  by  $\omega_c$ .

## 4. Results and discussion

### 4.1. Mapping morphological dimensionless ratios

Dimensionless ratios in ephemeral channels are conditioned by very diverse factors, including the relative location and morphological features of riffles and pools, local rocky bed outcrops, and the erodibility of banks. Insinuous and meandering gravel-bed stretches, the pools are preferentially located on the bends and the riffles at the inflection points, but rocky substrate outcrops and erodible banks often show a less distinct spatial distribution. The bankfull channel in this study is characterized by intermediate width-to-depth ratios along the different stretches (Fig. 7).

Usually, channels with point bars are significantly wider at bendways than at crossings. In our case, well-developed point bars are

present around the bend apex but highly erosion-resistant banks and narrow pools here restrict the widening of the channel. Moreover, erodible banks, composed of marl and silt, and rocky bed outcrops (loamy limestone substrate) are more frequent, although somewhat discontinuous, along straight and slightly sinuous sections. This explains why the average WDR was even lower in BS (18.33) than in SS (20.59), with standard deviations of 6.77 and 9.05, respectively (Table 1). The higher variability observed in SS is because of a greater alternation of changes in channel width associated with transitions from alluvium to bedrock. The channel segments from the inflection point to the meander bend apex (IP-MBA) showed an average WDR slightly higher than that estimated for BS, increasing downstream from the bend apex to the inflection point (MBA-IP) (mean WDR of 19.48), where gravel riffles become large and stable. Nonetheless, the  $W_a/W_i$  and  $W_p/W_i$  ratios ranged from 1.10 to 1.42 and from 0.90 to 1.24, respectively, both being independent of the sinuosity, which is consistent with the results found by the NRCS (2007b) for this channel planform.

A pattern similar to that of the WDR is observed in the IR values, the average values in bends being lower than in straight sections and very similar to those of stretches from inflection points to bend apices. In addition, in this case, the highest incision ratios were recorded in the SS and downstream from the bend apex to the inflection point (MBA-IP), with average values of 2.39 and 2.21, respectively, for IR (low) and around 2.50 in both types of stretch for IR (upp). Such data reveal a difference in recent geomorphological behavior between straight stretches and bends. Despite showing both moderate WDR and highly incised cross sections, the incision in SS was accompanied by greater bank erodibility and channel widening than in BS, associated with a more extensive presence of detached blocks from the banks, exhumed old and thick sediments, and rocky bed outcrops. The MBA-IP sections exhibited the same trends as the IP-MBA, but in this case, the average incision values depended more on the pool length and bed scouring when leaving the bend, while the bankfull channel becomes wider according to differential erosion of lateral gravel bars in contact with soft bank materials. The ER followed a different pattern. The straight channel stretches are the most entrenched and hardly have adjacent floodplains, while the average ER was more moderate in bend sections. This behavior, compared to the spatial patterns found for WDR and IR, suggests that, at bankfull stage, the current channel adjustments are somewhat different from those produced in the past. Although the incision rate has always been high since the initial configuration of the lowest bank, it is currently being reduced because of a greater bed resistance to erosion.

### 4.2. Stream power maps

Fig. 8 shows the flow velocity ( $v$ ), shear stress ( $\tau$ ) and stream power ( $\omega$ ) estimated continuously along the bankfull channel. These values allowed us to infer the reach boundaries that were then related to the spatial patterns of DMR in order to better elucidate the processes that shape the channel. The reach flow velocity ranged from  $0.43\ m\ s^{-1}$ , for the widest stretch, to  $2.67\ m\ s^{-1}$ , for the narrowest cross section. Specifically, the greatest increases in flow velocity were in the steepest and narrowest stretches, confined within bedrock boundaries, because flow feedbacks operating in the alluvial bed areas do not occur here. This agrees with Finnegan et al. (2005), who suggested that a stream tends to maintain a narrower channel in bedrock than in gravel at the same discharge. Furthermore, because  $\omega(i)$  results from the multiplication of  $v$  by  $\tau$  for a given cell  $i$ , the spatial pattern of  $\omega$  reflected a large variability in the values, because of fluctuations of both variables. In this study, the shear stress varied from  $9.5$  to  $614.4\ N\ m^{-2}$  and the mean stream power from  $4.2$  to  $1509.8\ W\ m^{-2}$  (the upper limits of color displayed in Fig. 8 for such variables encompass the 95% of the data, that is  $455\ N\ m^{-2}$  and  $981.5\ W\ m^{-2}$  respectively).

As in the case with the flow velocity, the highest values of shear stress and mean stream power were concentrated in entrenched channel cross sections, along straight to sinuous sub-reaches and locally at

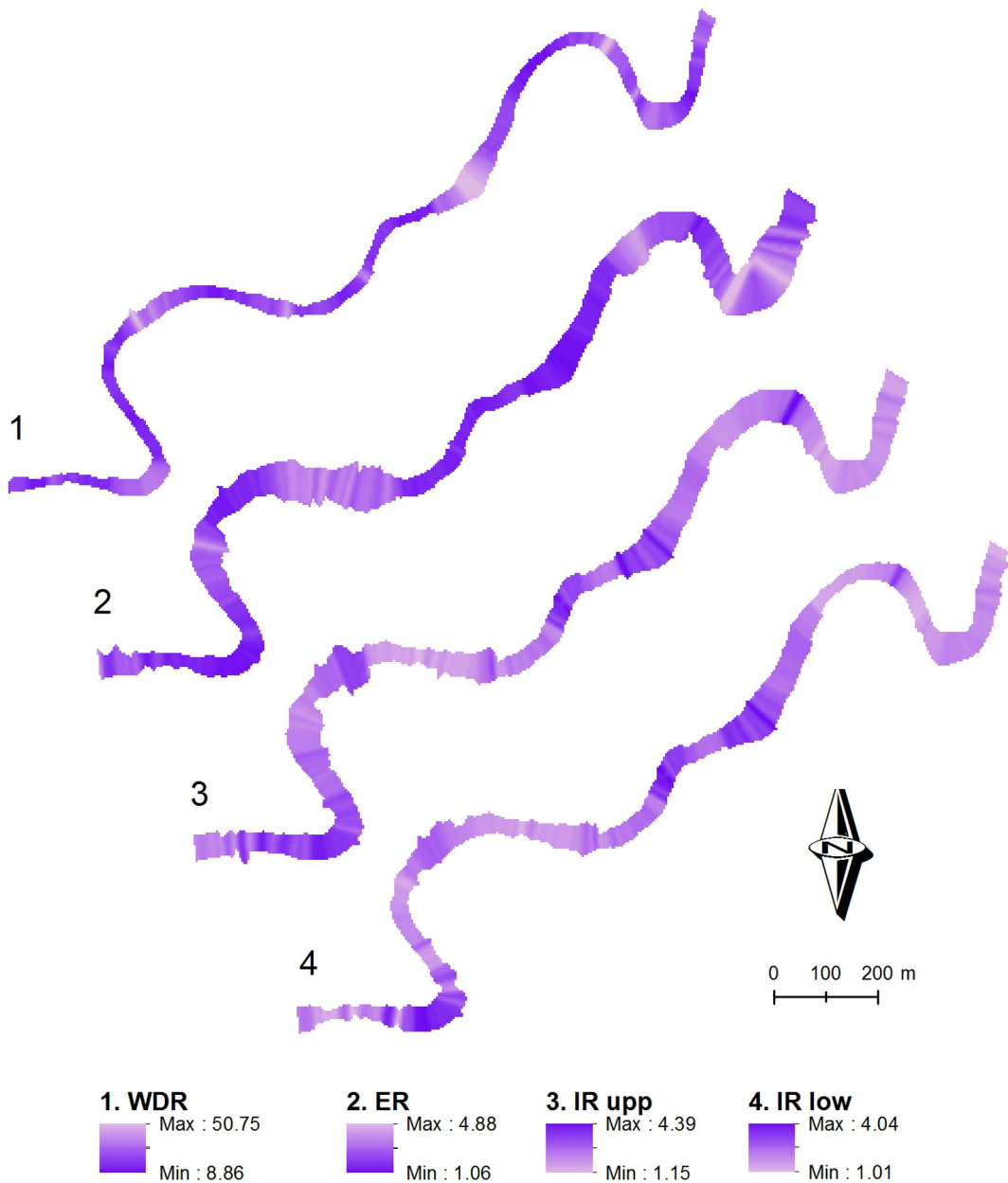


**Fig. 7.** Dimensionless ratios (WDR, ER, IR<sub>upp</sub> and IR<sub>low</sub>) obtained for each cell by spatial interpolation of geometrical data related to channel cross sections spaced at a distance of 10 m.

the entrance of sharp meander bends. This pattern is framed within an overall tendency towards incision pointed out by other authors in several streams in Mediterranean semi-arid conditions (e.g., Garzón and Alonso, 2002, Hooke, 2006, Ortega et al., 2014). However, we also observed significant width changes in slightly sinuous bedrock stretches with shear stress values below 100 N m<sup>-2</sup>, which is consistent with the results of Krapesch and Habersack (2011).

**Table 1**

Mean values and standard deviations calculated for different dimensionless ratios in each stretch class and considering the whole channel reach (WCR).

DMR	BS		SS		IP-MBA		MBA-IP		WCR	
	Mean	$\sigma$	Mean	$\sigma$	Mean	$\sigma$	Mean	$\sigma$	Mean	$\sigma$
WDR	18.33	6.77	20.59	9.05	18.83	7.36	19.48	8.12	19.19	7.75
ER	2.09	0.76	1.63	0.59	1.87	0.71	1.98	0.75	1.92	0.73
IR (upp)	2.34	0.67	2.50	0.67	2.33	0.59	2.48	0.75	2.40	0.67
IR (low)	2.00	0.65	2.39	0.71	2.07	0.54	2.21	0.83	2.13	0.70

The fact that the spatial pattern of  $\omega$  faithfully reflects those of  $v$  and  $\tau$  is because of the high correlation between  $v$  and  $\tau$ . From the results of regression equations and the corresponding coefficients of determination for the relationships between bankfull flow velocity ( $v_{bf}$ ) and other hydraulic variables (Fig. 9), it is verified that both variables, velocity and shear stress, had an excellent fit with a power function ( $r^2 = 0.92$ ). Only the Froude number has a higher correlation with velocity when fit with a linear function ( $r^2 = 0.96$ ). The  $v_{bf}$  values also showed a very good fit with the energy slope ( $r^2 = 0.90$ ), but a weaker relationship with the hydraulic radius ( $r^2 = 0.54$ ), and a very weak relationship with the maximum bankfull depth ( $r^2 = 0.19$ ).

#### 4.3. Relationships between dimensionless ratios and morphological parameters at bankfull stage

Dimensionless ratios based on empirically derived relationships between morphometric parameters referring to bankfull channel cross sections provided varied results throughout the reach. The degree of

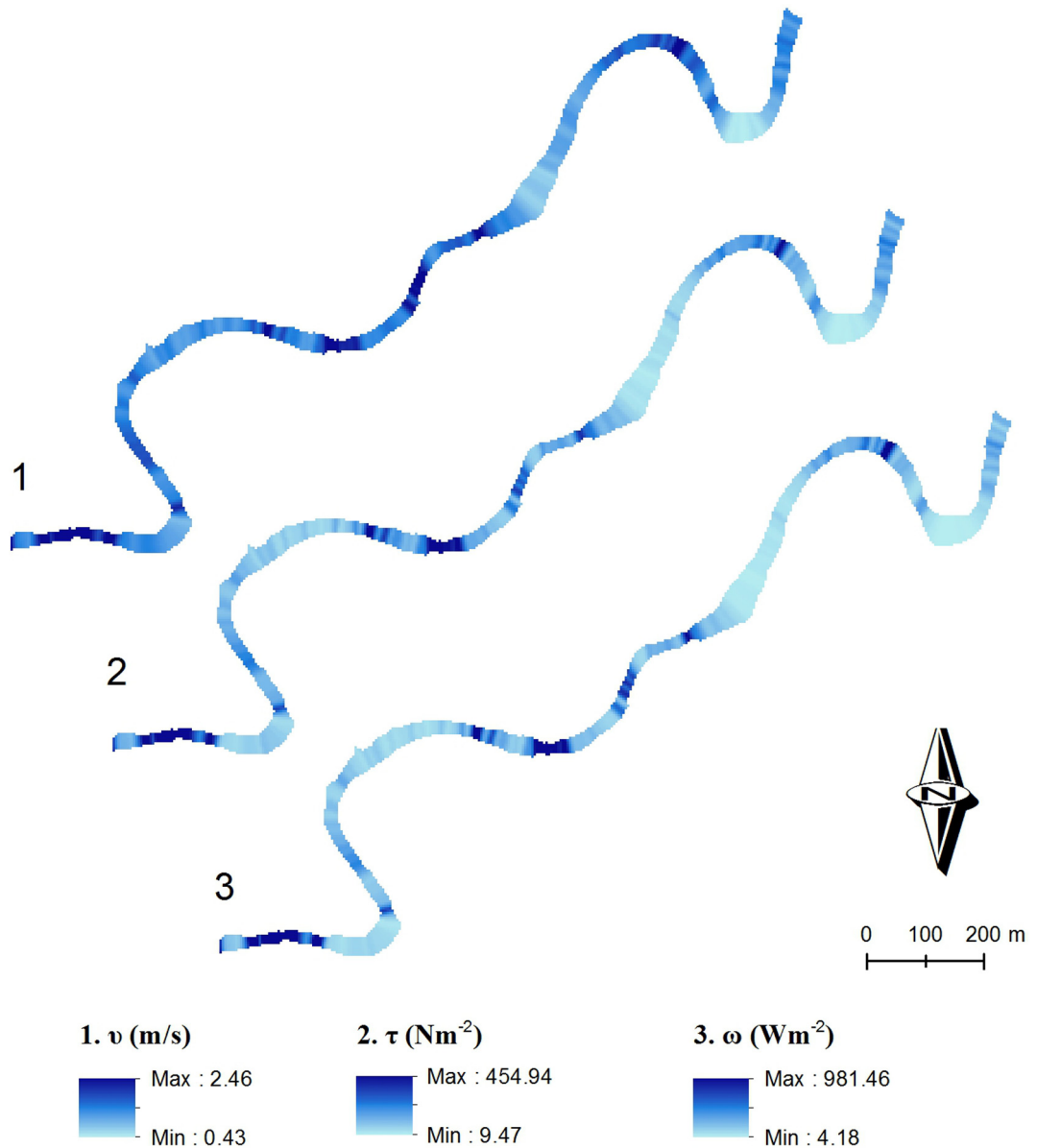


**Fig. 8.** Values of  $v$ ,  $\tau$ , and  $\omega$  obtained for each cell by spatial interpolation of Hec-RAS data related to equally spaced (10 m) bankfull cross sections. Maximum color limits represent the 95% of their respective data sets.

entrenchment displayed weak to moderate relationships with bankfull geometry and channel hydraulic variables, in contrast to the results obtained by other authors in perennial streams draining rainy mountain catchments. Specifically, Luebke (2006) found moderate to strong relationships between both types of parameters for different streams located in the Blue Ridge Mountains of western North Carolina and northern Georgia. In our study reach (the Upper Mula stream), the entrenchment ratio (ER) showed a very low correlation with the bankfull dimensions. These differences are not generalizable because some factors that control the bankfull hydraulic geometry can vary from one location to another, regardless of the flow regime. In the cases of perennial mountain streams, the current bankfull conditions often reflect the variability in flow dynamics within riffle-pool sequences, which dominated the entire entrenchment stage. In contrast, some ephemeral channels (e.g., the Upper Mula stream) are currently characterized by an increase in bed armoring and local rocky outcrops. Consequently, the previous entrenchment rate here tends to be interrupted, denoting a significant change in the bankfull channel geometry and a weaker relationship with the ER. For the whole series of ER values, moderate relationships

were observed with the incision ratios ( $IR_{upp}$  and  $IR_{low}$ ), the maximum bankfull depth ( $MD_{bf}$ ) and the flood prone width ( $W_{fp}$ ), with  $r^2$  values ranging from 0.48 to 0.53. However, the relationships between the ER and  $W_{fp}$ , hydraulic depth ( $H_d$ ) and channel width at bankfull stage ( $W_{bf}$ ) were insignificant, providing a coefficient of determination  $<0.2$ . In fact, the development of the floodplain adjacent to the current active channel often coincided with an increase in the maximum bankfull depth, depending on the cross-sectional geometry and the sub-reach planform.

The dimensionless ratios for the cells meeting the criteria in Table 2 were compared to each other and with the geomorphic dimensions (e.g.,  $W_{bf}$ ,  $H_d$ , LBH,  $W_{fp}$  and  $MD_{bf}$ ) from which they were derived at cell i (Fig. 10 and Table 3). The results show very different relationships in many cases, denoting the succession of channel stretches of contrasting and transitional forms. The lack of uniformity in the physical characteristics of this stream reach does not result just from the stretch classes as a function of the channel curvature and the transect between the inflection point and meander bend apex. Spatial changes in inextricably linked variables,

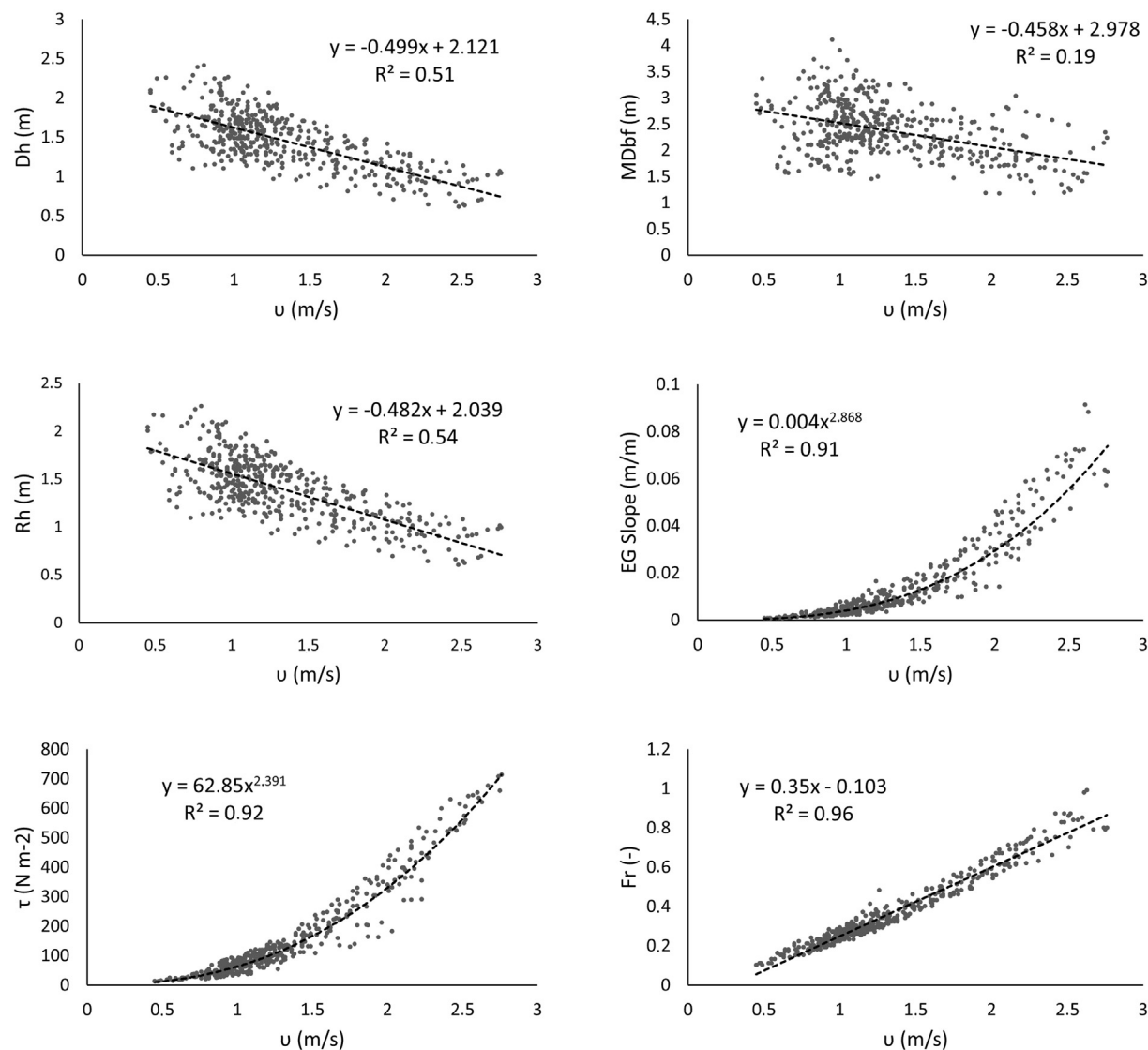


**Fig. 9.** Relationships between bankfull flow velocity ( $u_{bf}$ ) and other hydraulic variables (hydraulic depth, maximum bankfull depth, hydraulic radius, energy slope, shear stress and Froude number) at the significance level ( $p$ -value) < 0.05.

such as roughness, bed material, and grain size also play a relevant role in morphological adjustments.

Cross sections with a more shallow thalweg were located in the more entrenched straight sub-reaches (Fig. 10), possibly because of

rock outcrops in most of them after previous phases of greater incision. In these cases, the maximum bankfull depth potentially decreased with the degree of entrenchment so that in the most embedded cross sections it barely exceeded 1.5 m (Table 3). Less frequent were the low  $MD_{bf}$  recorded in curved channel sub-reaches with high entrenchment. Moderately entrenched stream sections and those exhibiting negligible or no entrenchment showed a different pattern: in both cases, a clear increase in the  $MD_{bf}$  and a preferred location of bed scour in the meander bends were noted. The  $MD_{bf}$  values ranged from 1.5 to 3 m in the meander cross sections with moderate ER, and from 2 to 3.7 m along slightly entrenched bends (Fig. 10). In this type of stretch, a better fit and positive relationship were observed between  $MD_{bf}$  and ER ( $r^2 = 0.54$ ). For the cross sections belonging to straight stretches (SS), slightly or moderately entrenched, the relationships between ER and  $MD_{bf}$  were weak.

Variations within and among these sub-reaches may also be caused by the uncertainty in the field measurements when applying the criteria used to identify the bankfull level and the lowest bank height along entrenched and non-entrenched stretches. As previously reported (Simon and Darby, 1997; Juracek and Fitzpatrick, 2003; Luebke, 2006), it is assumed that the bankfull level in entrenched sections can create errors in the computation of the Rosgen entrenchment ratio when this is extrapolated from the tops of point bars or flood scars. The

**Table 2**

Cases and stream types defined from different ranges of dimensionless ratios (WDR, ER, and IR).

Dimensionless ratio	Case/category	Stream type
Width/Depth Ratio (WDR)	(1)WDR < 12	Streams with low W/D ratio
	(2)12 < WDR < 24	Streams with moderate W/D ratio
	(3)24 < WDR < 40	Streams with moderate to high W/D ratio
	(4)WDR > 40	Streams with very high W/D ratio
Entrenchment Ratio (ER)	(1)ER < 1.4	Highly entrenched streams
	(2)1.4 < ER < 2.2	Moderately entrenched streams
	(3)ER > 2.2	Streams exhibiting low or no entrenchment
Incision Ratio (IR)	(1)IR < 2	Moderately incised streams
	(2)2 < IR < 3	Highly incised streams
	(3)IR > 3	Very highly incised streams

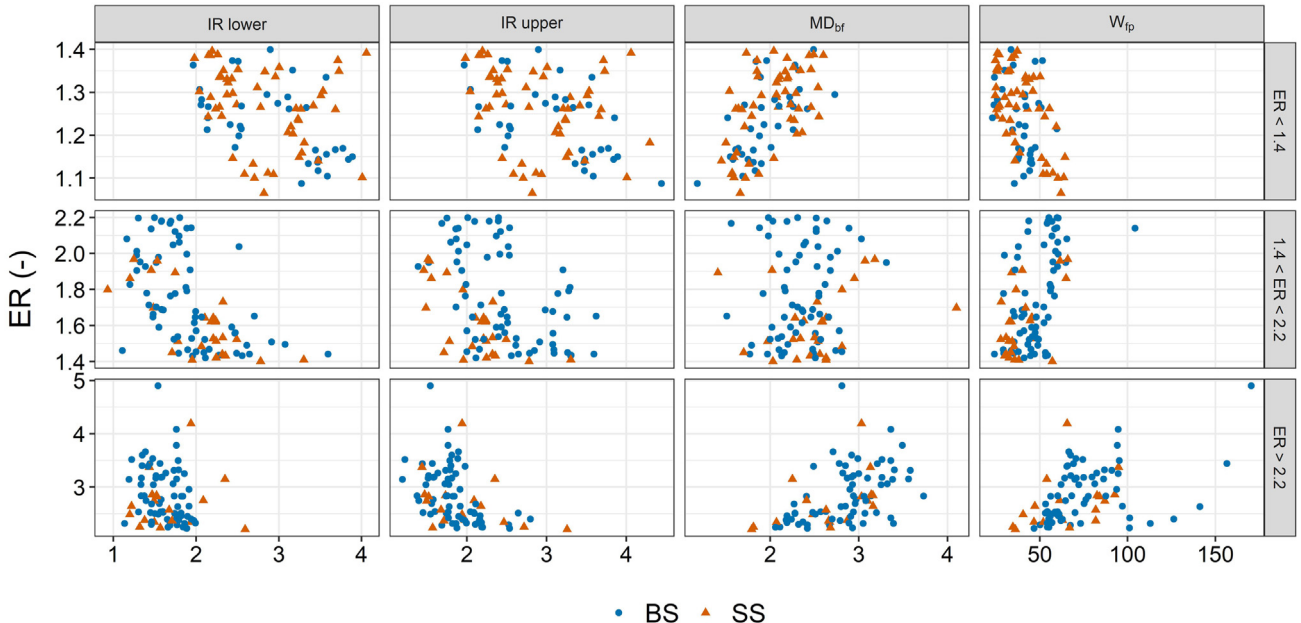


**Fig. 10.** Comparison of cell values included in each range of ER (see Table 2) with those of other morphological variables having a stronger correlation ( $r^2 > 0.5$ ) for the whole stream reach.

entrenchment ratio therefore seems to be a less consistent variable here than when used to discriminate intermittent from perennial streams (Ken et al., 2008).

The equations determining the most significant relationships between dimensionless ratios and bankfull channel metrics were mainly best described by power functions (Table 3). This agrees with the findings of numerous researchers who related morphological channel dynamics to changes in bankfull geometry using non-linear functions that become asymptotic and reach minimum variance with time (Simon and Rinaldi, 2006).

#### 4.4. Comparison of stream power with bed stability indicators and dimensionless ratios

In general, incision occurs when the boundary shear stress and stream power overcome the strength of the bed materials (Harvey and Watson, 1986). By comparing the map of stream power (Fig. 8) with the spatial distribution of bedforms, bed stability indices, and incision ratios, we explored whether the stream power thresholds set by other authors (e.g., Brookes, 1987; Magilligan, 1992; Stacey and Rutherford, 2007) in perennial, gravel-bed streams are valid for the ephemeral streams in semi-arid environments (first hypothesis, Section 1). In our case, a high spatial variability of bedforms and grain sizes was observed, leading to stability changes over relatively short distances and also affecting the stream power required for transport. These authors proposed stream power thresholds  $35 \text{ W m}^{-2}$  for riverbed

erosion and  $300 \text{ W m}^{-2}$  for significant channel morphological changes. Such thresholds and intermediate phases of minor undercutting and local bed scour have already been widely applied in stream rehabilitation works. According to such considerations, cross sections with an unstable bed would have stream powers above  $35 \text{ W m}^{-2}$ , whereas stable bed locations would have lower stream powers. This threshold of stability was not detected in many of the cross sections studied here (Table 4). Around 33% of the cross sections showed an efficient transport capacity, with  $\tau$  values above their respective  $\tau_c$  estimated from  $D_{84}$  (RBS < 1), and 67% of them experienced bed stability (RBS > 1) (Table 4).

Nevertheless, the difference between the mean  $\omega$  of stable and unstable beds along the entire channel reach was not always significant, which is consistent with the results found by Stacey and Rutherford (2007). Based on the fundamentals of driving forces and sediment transport, we hypothesise that the  $\omega$  required to initiate transport will vary with particle size and bedforms. In no case did the threshold of  $35 \text{ W m}^{-2}$  coincide with the limit defined by the "relative bed stability" (RBS) index. Furthermore, if we consider moderately incised stream stretches ( $1 < \text{IR} < 2$ ) and other, highly incised ones ( $\text{IR} > 2$ ), the minimum  $\omega$  thresholds required to move the coarsest surface particles ( $D_{84}$ ) and generate bed scouring were very similar (87.5 and  $88.3 \text{ W m}^{-2}$ , respectively). In contrast, the minimum  $\omega$  thresholds associated with the most active bedforms were found to be lower, specifically between 12 and  $35 \text{ W m}^{-2}$  in 19.3% of cases with BFS < 0.5 for  $1 < \text{IR} < 2$  and between 7 and  $36 \text{ W m}^{-2}$  in 33.3% of sites with the same BFS range for  $\text{IR} > 2$ . Such differences could be related in part to the increased presence of erosion resistant bedforms in the sub-reaches with moderate incision than in the most highly incised ones, where the active bars predominate (Table 5). Above these minimum thresholds, the interval of  $\omega$  commonly associated with moderate to significant morphological changes in perennial gravel-bed streams ( $35\text{--}300 \text{ W m}^{-2}$ ) showed different patterns here in terms of frequency and magnitude. In less incised cross sections, the percentage of cases within this range (40.2%) was higher than in the most incised ones (35.1%). However, the patterns of the magnitude of  $\omega$  in both types of section were different depending on whether the RBS index or the BFS was applied.

I(IR) = IR interval; RG = RBS or BFS range for which  $\omega$  (mean stream power) values are calculated; I( $\omega$ ) =  $\omega$  interval; Fq = Frequency of channel cross-sections with SP within each I( $\omega$ ); % T = percentage of the number of cases in each  $\omega$  interval with respect to total

**Table 3**

Significant relationships between dimensionless ratios and morphological parameters at bankfull stage for different stretch classes.  $p$ -Value < .05 at the confidence interval of 95%.

Stretch cases	ER vs IR, MD <sub>bf</sub> & W <sub>fp</sub>	IR, MD <sub>bf</sub> & W <sub>fp</sub> vs ER	$r^2$
SS (1.4 < ER < 2.2)	ER = $1.94 \text{ IR}_{\text{low}}^{-0.28}$	$\text{IR}_{\text{low}} = 3.13 \text{ ER}^{-0.99}$	0.51
SS (1.4 < ER < 2.2)	ER = $2.15 \text{ IR}_{\text{upp}}^{-0.40}$	$\text{IR}_{\text{upp}} = 3.20 \text{ ER}^{-0.62}$	0.51
BS (ER < 1.4)	ER = $1.03 \text{ MD}_{\text{bf}}^{0.27}$	$\text{MD}_{\text{bf}} = 1.45 \text{ ER}^{1.37}$	0.42
BS (ER > 1.4)	ER = $0.66 \text{ MD}_{\text{bf}}^{0.24}$	$\text{MD}_{\text{bf}} = 1.80 \text{ ER}^{0.43}$	0.54
BS (ER)	ER = $3.39 \text{ IR}_{\text{low}}^{-0.84}$	$\text{IR}_{\text{low}} = 2.84 \text{ ER}^{-0.59}$	0.50
BS (ER)	ER = $4.41 \text{ IR}_{\text{upp}}^{-0.99}$	$\text{IR}_{\text{upp}} = 3.41 \text{ ER}^{-0.61}$	0.61
SS (ER)	ER = $2.62 \text{ IR}_{\text{low}}^{-0.64}$	$\text{IR}_{\text{low}} = 3.11 \text{ ER}^{-0.72}$	0.47
SS + BS (ER)	ER = $3.19 \text{ IR}_{\text{low}}^{-0.80}$	$\text{IR}_{\text{low}} = 2.96 \text{ ER}^{-0.64}$	0.52
SS + BS (ER)	ER = $3.91 \text{ IR}_{\text{upp}}^{-0.92}$	$\text{IR}_{\text{upp}} = 3.22 \text{ ER}^{-0.56}$	0.53
SS + BS (ER)	ER = $0.68 \text{ MD}_{\text{bf}}^{1.14}$	$\text{MD}_{\text{bf}} = 1.82 \text{ ER}^{-0.43}$	0.48
SS + BS (ER)	ER = $0.024 \text{ WFP} + 0.64$	$\text{WFP} = 21.48 + 11.22 \text{ ER}^{-0.43}$	0.48

**Table 4**  
Basic statistics obtained for  $\omega$  from different ranges of IR and bed stability indices (RBS and BFS), using the stream power thresholds proposed by Magilligan (1992) and Stacey and Rutherford (2007) to evaluate the capacity for morphological adjustment in perennial, gravel-bed streams.

I(IR)	IR < 2		IR > 2	
	RG	BFS < 1	RBS < 2	BFS < 0.5
$\omega$ for RBS < 1	<35	>300	<35	>300
Fq	0	24	4	0
% T	0	15.2	4.6	0
% R	0	19.7	0.8	22
% SP	0	76.9	23.1	22.7
Min	-	87.5	303.9	96.7
Med	-	146.9	788.3	35.2
$\sigma$	-	52.1	514.9	4.5
$\omega$ for BFS < 1	<35	>300	<35	>300
Fq	22	90	2	28
% T	4.2	17.1	0.4	5.3
% RG	0	21.6	79	1.8
% SP	19.3	79	1.8	16.9
Min	12.2	35.6	749.6	4.5
Med	27.4	83.6	749.6	16.1
$\sigma$	6.5	363	0	11
IR < 2				
$\omega$ for RBS < 1	<35	>300	<35	>300
Fq	24	116	40	0
% T	0	4.6	0	0
% R	0	0.8	0	0
% SP	0	22	0	0
Min	-	0	0	0
Med	-	0	0	0
$\sigma$	-	0	0	0
IR > 2				
$\omega$ for RBS < 1	<35	>300	<35	>300
Fq	22	116	40	0
% T	0	4.6	0	0
% R	0	0.8	0	0
% SP	0	22	0	0
Min	-	0	0	0
Med	-	0	0	0
$\sigma$	-	0	0	0

of cases in the entire channel reach; %  $\omega$  = percentage of the number of cases in each  $\omega$  interval with respect to total of cases in each RBS or BFS range. Min, Med and  $\sigma$  = Minimum, median and standard deviation values of  $\omega$  for each I( $\omega$ ) within each RBS or BFS range.

If the RBS is used as a stability criterion, two  $\omega$  patterns are observed with very different statistics for stable and unstable beds, regardless of the degree of incision: (1) a pattern of unstable granular beds (RBS < 1) whose median  $\omega$  is around  $150 \text{ W m}^{-2}$ , with  $\sigma$  from 52.1 to 64.1; and (2) a relatively stable bed pattern, whose median  $\omega$  and  $\sigma$  decrease as the degree of stability increases. On the other hand, the patterns related to the magnitude of the  $35\text{--}300 \text{ W m}^{-2}$  range reflect the different incision ratios. In the less incised sub-reaches, the median  $\omega$  within this range affecting more unstable bedforms (BFS < 0.5) is much lower than that estimated under conditions of greater morphological stability (BFS > 0.5). In contrast, such differences between the statistics of  $\omega$  corresponding to the relatively stable and unstable bedforms are not significant in the highly incised sub-reaches. Regarding the threshold associated with the higher erosion rates, there was a correspondence between  $\omega$  values  $>300 \text{ W m}^{-2}$  and the highest values of the bed instability indices. The threshold of  $300 \text{ W m}^{-2}$ , suggested by Magilligan (1992) for major morphological adjustments with erosion, was exceeded in 16% of cases, although about a third of that percentage occurred in sections with a very stable bed (Table 4). These stable beds are usually characterized by local outcrops of rocky substrate or are composed of coarse pebbles and blocks that are presumed to be mobilized only in large events. In these cases, a clear influence of bed armoring on channel stability was observed, as found by other authors (Wittenberg et al., 2007; Conesa García and García Lorenzo, 2007) in Mediterranean ephemeral gravel-bed streams.

The values of  $\omega(i)$  were related to RBS( $i$ ) and BFS( $i$ ) for each stretch class (Fig. 11) in order to test the second hypothesis (Section 1). The largest values of RBS ( $\tau_c/\tau_0 > 4$ ) occurred where  $\omega$  approaches zero, mainly in the IP-MBA, BS, and transitional sub-reaches from SS to BS, while the greater bankfull flow competence ( $\omega > 300 \text{ W m}^{-2}$ ) affected MBA-IP channel stretches with an unstable granular bed (RBS < 1) (Fig. 11).

However, the patterns of variation of  $\omega$  coincided less with those of BFS. In the straight stretches, there was a greater correspondence between the variations of  $\omega$  and BFS, rather than in bend channel sections, and here decreases in  $\omega$  were often accompanied by increases in BFS. The correlation between  $\omega$  and BFS was highest above the threshold of  $270 \text{ W m}^{-2}$ , and was unaffected by the degree of sinuosity, channel planform and distance from the meander bend apexes (Fig. 11). This occurs because the more stable bedforms (BFS > 0.5) along the channel centerline (e.g., rocky substrate outcrops and exhumed old coarse-grained sediments), prevail in narrower bankfull cross sections with greater slope and shear stress than those dominated by active bars. In fact, the locational weight estimated for bedrock areas in straight sub-reaches with a low WDR (<12) ( $LW_{bgu} = 0.35$ ) was much higher than that obtained for active bar areas within the same WDR interval ( $LW_{bgu} = 0.18$ ) (Table 5). The active bedforms were well represented in all the classes of channel stretches, but were more abundant at sites with a moderate to very high WDR (>24) ( $0.49 < LW_{bgu} < 0.57$ ) and a high incision ratio (IR > 2) ( $0.38 < LW_{bgu} < 0.58$ ). At sites with moderate to very high WDRs, active bars are mobile and frequently changing, while sites with a high IR experience sediment feedbacks and gradual bed accretion that may be associated with sites that have undergone a deep incision in the past. The locational weight of the active and vegetated bars was not a discriminant indicator of the class of stretch (Table 5). Riffles and steps had the highest  $LW_{bgu}$  values in runs within incised channels, stream cross sections with very high WDR along transitions from alluvium to bedrock, and stretches from inflection points to meander-bend apices.

Box plots relating  $\omega/\omega_c$ ,  $\partial\omega/\partial s$ , and BFS to different IR and WDR categories are displayed in Fig. 12. To verify the third and fourth hypothesis (Section 1), this analysis yielded different patterns of energy balance

**Table 5**

Locational weight values of the bed geomorphic units ( $LW_{bgu}$ ) in each channel stretch class and for different incision (IR) and width-to-depth (WDR) ratios.

Bed geomorphic units (bgu)	IR (1)	IR (2)	IR (3)	WDR (1)	WDR (2)	WDR (3)	WDR (4)	BS	SS	IP-MBA	MBA-IP
Active channel	0.15	0.18	0.16	0.31	0.15	0.11	0.09	0.15	0.18	0.14	0.18
Active bars	0.27	0.38	0.58	0.18	0.33	0.49	0.57	0.37	0.33	0.35	0.36
Vegetated bars	0.37	0.26	0.15	0.32	0.31	0.28	0.23	0.30	0.30	0.33	0.27
Bank failure deposits	0.03	0.04	0.07	0.03	0.04	0.04	0.03	0.04	0.03	0.03	0.05
Riffles and steps	0.22	0.38	0.23	0.12	0.30	0.27	0.41	0.28	0.27	0.32	0.22
Pools and point bars in bends	0.07	0.04	0.27	0.01	0.07	0.24	0.00	0.14	0.00	0.08	0.10
Bedrock and pools in straight reaches	0.12	0.17	0.12	0.35	0.13	0.00	0.00	0.11	0.18	0.09	0.18

Note: numbers in shaded cells refer to the cases/categories of the DMR defined in Table 2.

and power gradient in relation to the bed form stability within the ranges of incision and width-to-depth ratios referenced in Table 2.

The values of  $\omega/\omega_c$  were also skewed for most ranges of the WDR, with their medians decreasing as the WDR increased. In contrast to the pattern observed for the IR ranges, both BFS and  $\partial\omega/\partial s$  varied with

the WDR, at least up to the WDR threshold of 40, with the median  $\partial\omega/\partial s$  decreasing (1.5 to  $-1 \text{ W m}^{-2}/\text{m}$ ) and the median BFS increasing (0.46–0.57). Where BFS indices were  $>0.5$ , values of  $\partial\omega/\partial s$  were negative (Fig. 12). In addition, the data on the stability of the bedforms in relation to the width-to-depth ratio were more normally distributed than

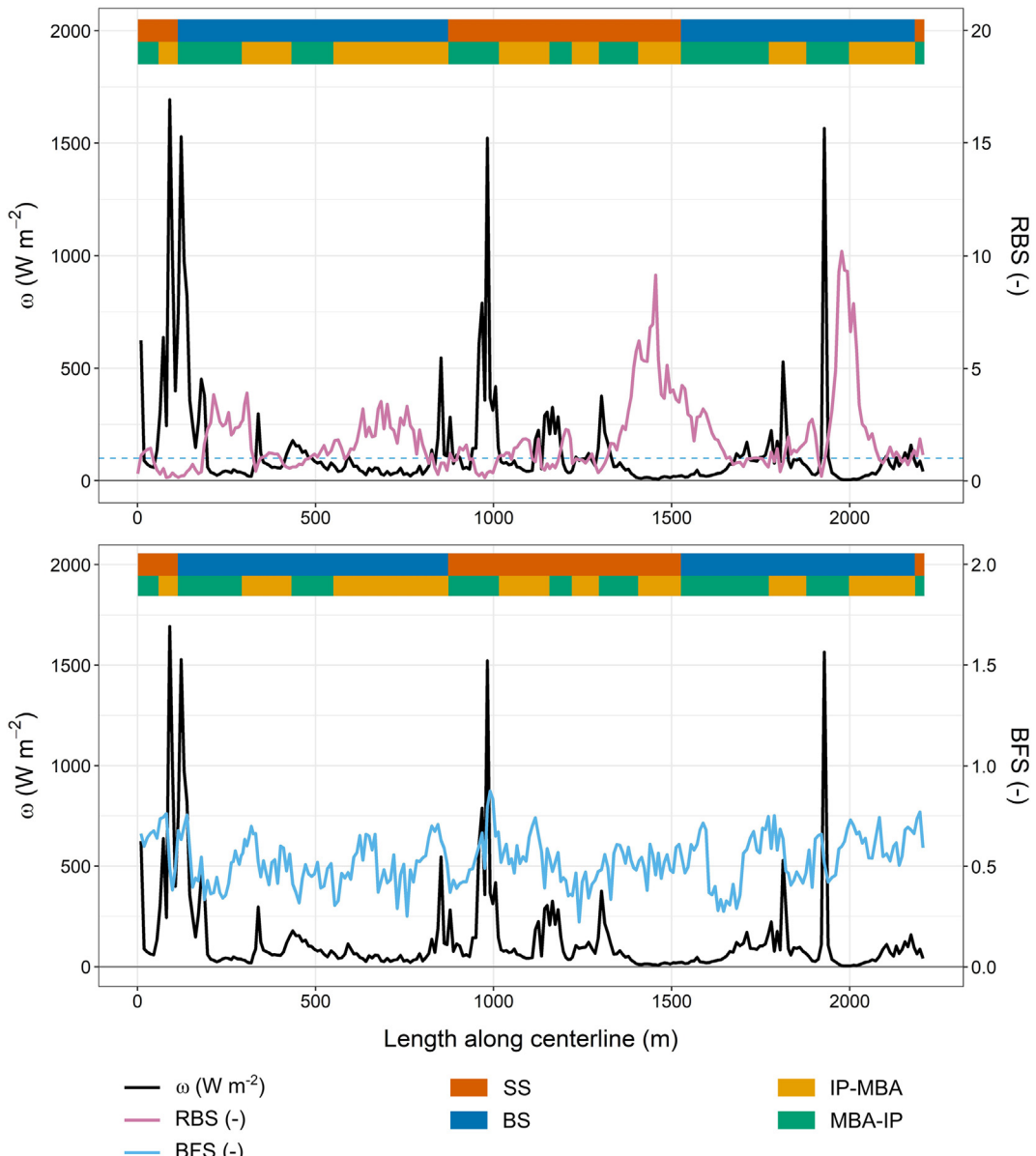


**Fig. 11.** Values of  $\omega(i)$  versus  $RBS(i)$  and  $BFS(i)$  for each stretch class along the channel centerline in the study reach.

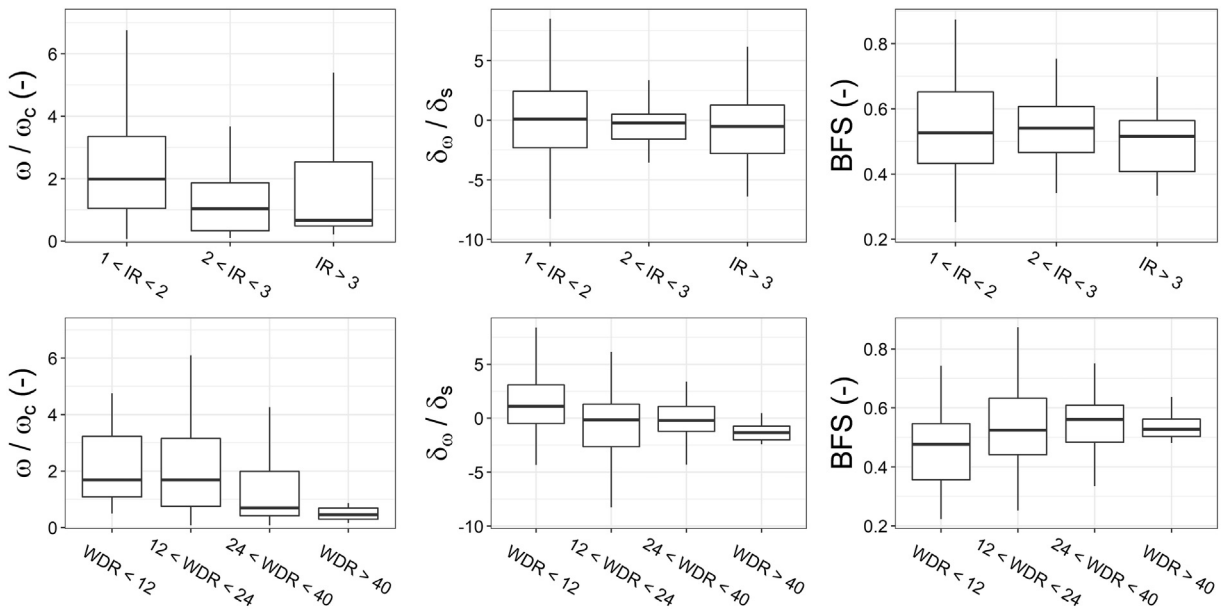


**Fig. 12.** Box plots showing the mean stream power gradient ( $\delta\omega/\delta s$ ), energy balance ( $\omega/\omega_c$ ), and BFS at bankfull level compared with different incision and width/depth ratios.

those for the power gradient. In both cases, the most closely grouped values between Q1 and Q3 occurred for sites with  $WDR > 24$ , where  $\delta\omega/\delta s$  reached values of 1.3 to  $-2.4$  and for BFS values of 0.47–0.62.

#### 4.5. Patterns of bankfull stream power and dimensionless ratios for different stretch classes

The relationships between  $\omega/\omega_c$  and  $\delta\omega/\delta s$  from different ranges of the DMR were obtained for each stream stretch class (Fig. 13). Our analyses indicate that two a priori patterns of bankfull stream power differed significantly depending on the stretch type and the DMR. The pattern found in bend stretches was characterized by a dense grouping of cross sections belonging to case 2 of the WDR, case 1 of the IR, and case 3 of the ER around low ranges of  $\omega/\omega_c$  and  $\delta\omega/\delta s$  ( $-1.5 < \omega/\omega_c < 2$ ;  $-2 < \delta\omega/\delta s < 1.5 \text{ W m}^{-2}/\text{m}$ ). That is, moderately incised cross sections, exhibiting negligible or no entrenchment and moderate W/D ratios along BS sub-reaches, were frequently subject to bankfull

discharges with low to moderate sediment-transporting capacity, causing bed stability and minor morphological adjustments. Higher energy balance values were more dispersed and tended to be located in less entrenched and less incised cross sections transitioning to channel widening.

For their part, the specific  $\omega/\omega_c$ – $\delta\omega/\delta s$  relationships in straight or slightly sinuous stretches (SS) showed a slightly different pattern: the lowest values of  $\omega/\omega_c$  and  $\delta\omega/\delta s$  (including negatives) were concentrated in stream cross sections representing cases 2 to 4 of the WDR, cases 2 and 3 of the IR and case 1 of the ER. By contrast, the extremely high values had preferred locations similar to those of the previous pattern, although they were increased in number and degree of dispersion. In this second spatial pattern, highly incised and entrenched cross sections with moderate to high width-to-depth ratio in straight stretches experienced high bed stability, little or no vertical erosion, and greater erosion of the highest bank. Generally, the critical stream power appears to be sensitive to the slope and grain size (Parker et al., 2011).

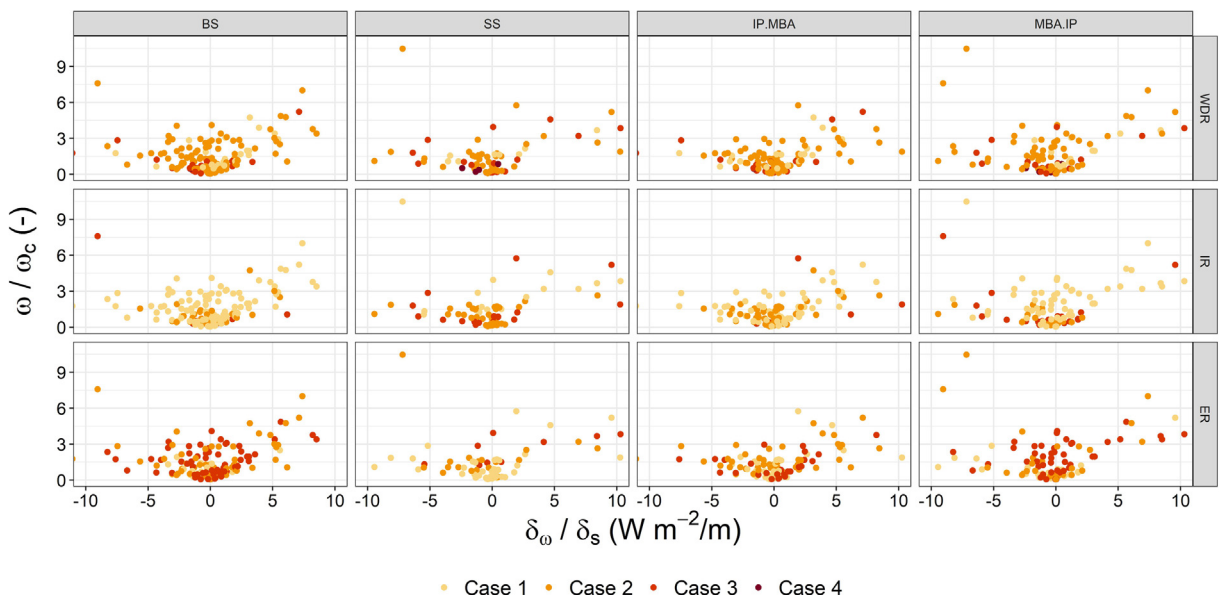


**Fig. 13.** Comparison of  $\omega/\omega_c$  and  $\delta\omega/\delta s$  for the cases of the dimensionless ratios (WDR, ER, and IR) defined in Table 2 in each stretch class (BS, SS, IP-MBA and MBA-IP).

Nevertheless, in granular-bed sites within this kind of stretch, changes in slope did not always lead to variations in  $\omega_c$  between cells because of the greater relative influence of grain roughness. Rickenmann and Recking (2011) and Camenen (2012) found similar results when studying the effect of the slope on the threshold of coarse-grain motion as a function of the Froude number and the relative flow depth. On the contrary, the most significant energy balances only occurred locally in the less entrenched stretches with moderate to high incision.

The  $\omega/\omega_c - \partial\omega/\partial s$  relationships obtained for the bend transects upstream and downstream from the meander apex had a distribution approximate to that observed for the BS (Fig. 13). However, the values in MBA-IP showed a greater dispersion than those in IP-MAB, especially in the case of cross sections with a moderate W/D ratio, where the riffles and steps occupied most of the bed.

Point clouds displaying the downstream change in the WDR and the IR in relation to the excess energy,  $\varepsilon$ , were plotted for channel cross sections with different bedforms in order to determine the spatial variability (Fig. 14) (see Hypothesis 5, Section 1). According to the sixth hypothesis, the relationships between  $\varepsilon$  at cell  $i$  and both DMR types at cells  $i$  and  $i + j$  were obtained to identify the trends and rate of change with distance, with 40 m as the length of each interval  $i + n$  ( $n = 4$  cells of 10 m resolution). This analysis revealed a lack of consistent, significant correlation between  $\varepsilon(i)$  and the IR or the WDR at any lag distance between 0 and 12 cells (from  $i$  to  $i + 3$ ) in all sections, regardless of the affected bedforms. Over similar ranges of  $\varepsilon$  at cell  $i$ , the width-to-depth ratio was lower on bedrock pools in straight stretches than on alluvial pools and point bars along bends, or on riffles and steps in intermediate sub-reaches. These results were not consistent across the entire straight

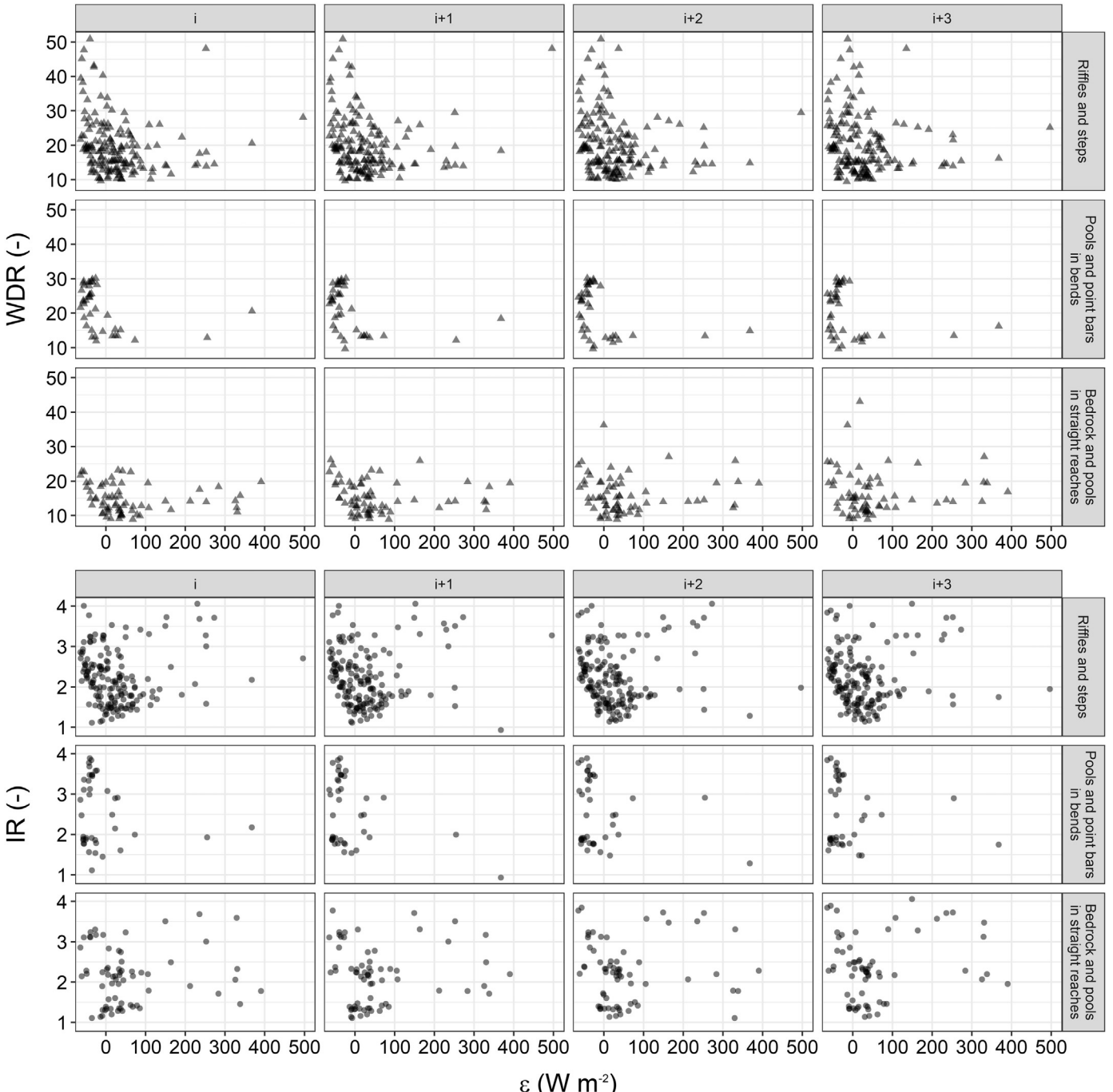


**Fig. 14.** Scatter plots comparing  $\varepsilon$  with IR and WDR at cells  $i$  and  $i + j$  for different bedforms (riffles and steps, pools and point bars in bends, bedrock and pools in straight reaches).

and bend subbreaches, where the highest values of the WDR occurred in SS along transitions from alluvium to substrate outcrop and vice versa. Therefore, the increase in the WDR and its degree of dispersion against  $\varepsilon(i)$ , as the lag interval increases, could be related to the presence of local bedrock pools in SS sites. In this case, a lag of  $i + 3$  implies an appreciable change in the WDR, which involves a strong variation in  $\varepsilon$  from the beginning. The influence of the rest of the bedforms on the spatial variability of the WDR downstream is less, given the limited variability observed in the point clouds representing the lag in each of the scatter plots. In fact, at sites with point bars and marginal pools the WDR(i) maximum (around 30) in relation to  $\varepsilon(i)$  was the same as for the cell  $i + 3$  (Fig. 14). The reference WDRs linked to a formative discharge (according to Sutfin et al., 2014), under conditions of bed stability (negative values of  $\varepsilon$ ), ranged from 7 to 23 for rocky substrate pools, from 11 to 30 for individual scroll bars and fine-grained pools, and from 10 to 50 along riffles and runs. In any case, the WDR does not define by itself the cross-sectional channel shape (Das, 2015) and the methodological limitations derived from it could also contribute to weak local relationships between this variable and the excess energy in the Upper Mula stream.

Such a pattern was not found for the relationships between the IR and  $\varepsilon$  as a function of the bedforms. The degree of dispersion in all the scatter plots did not vary substantially from  $i$  to  $i + 3$ . A few isolated sites recorded changes in the incision ratio for each lag interval that were marginally significant, although the loss of the effect of bedforms on that ratio was somewhat unequal in relation to  $\varepsilon(i)$ . The minimum IR value obtained for  $\varepsilon(i) < 100 \text{ W m}^{-2}$  in SS with bedrock pools increased from 1.1 at cell  $i$  to 1.5 at cell  $i + 3$ . However, a high bias remained, despite the under estimation of stream power variability, as already detected by Finnegan et al. (2005) in channels incising bedrock. In addition, variations in the excess of flow energy, associated with changes in erosional bed resistance, affected the transitional areas from alluvium to rock substrate.

In bend channel sites occupied by alluvial pools and point bars the minimum IR did not increase with the lag interval, but the frequency of moderately incised cross sections ( $1.5 < \text{IR} < 2$ ) did. The riffles and runs had very little influence on the incision ratio, at least for distances  $< 120 \text{ m}$ .

#### 4.6. Statistical dissimilarity among stretch classes

An ANOVA was performed in order to determine which variables explained the differences in behavior between the groups of each stretch class: straight stretches (SS) versus bend stretches (BS), and sections from the inflection point to the meander bend apex (IP-MBA) versus reaches from the meander bend apex to the inflection point (MBA-IP) (Table 6).

The results show that the variables RBS, BFS, and  $W_{bf}$  influenced in a non-significant way the differences between the SS and BS groups. The rest of the variables had a significant relationship, with the rejection of the null hypothesis of equality of variances, and therefore, it can be concluded that there are important differences between the SS and BS classes. These differences were influenced above all by the variables  $IR_{low}$ , ER and  $MD_{bf}$ . In this case, IR had the greatest impact (followed by ER) among the SS-BS groups, because of its greater sensitivity as a measure of bed degradation. The  $v$  and  $\tau$  also had a more moderate relationship because variations in the  $\partial\omega/\partial s$  ratio affected the stability to different degrees depending on the stretch planform and sinuosity. In addition, only the variable  $MD_{bf}$  had a non-significant relationship between the IP-MAB and MAB-IP classes ( $p < .05$ ) and influenced the spatial variability of both groups.

The relationships between  $\omega/\omega_c$  and  $\partial\omega/\partial s$  from different ranges of the DMR (IR and ER) showed greater similarity for the IP-MAB vs MAB-IP stretches than for those of BS vs SS. Levene's test was applied to guarantee the robustness of the ANOVA, and its results being

**Table 6**

ANOVA results for the stretch classes SS vs BS and IP-MAB vs MAB-IP from different hydraulic and morphological variables.

Variable	SS vs BS Groups				IP-MAB vs MAB-IP Groups			
	Sum.Sq	df	F-value	p-Value	Sum.Sq	df	F-value	p-Value
$v_{bf}$	1.054 39.72	1 263	6.98 6.78	0.0097 0.010	0.322 40.46	1 263	2.09 2.30	0.149 0.131
$\tau_{bf}$	$6.05 \cdot 10^4$ $2.35 \cdot 10^6$	1 263	6.78 5.28	0.010 0.022	$2.09 \cdot 10^4$ $2.39 \cdot 10^5$	1 263	2.30 2.10	0.131 0.148
$\omega$	$2.85 \cdot 10^5$ $1.42 \cdot 10^7$	1 263	5.28 5.38	0.022 0.021	$1.15 \cdot 10^5$ $1.44 \cdot 10^7$	1 263	2.10 2.00	0.148 0.158
$\partial\omega/\partial s$	0.0006 0.0291	1 263	5.38 5.38	0.021 0.0295	0.0002 0.0295	1 263	2.00 2.00	0.158 0.158
RBS	0.2637 775.2	1 263	0.09 0.09	0.765 0.765	1.460 773.9	1 263	0.50 0.50	0.482 0.482
BFS	0.0082 3.7620	1 262	0.57 0.57	0.450 0.450	0.032 3.738	1 262	2.24 2.24	0.135 0.135
IR <sub>low</sub>	9.293 118.8	1 263	20.57 20.57	<0.001 <0.001	1.257 126.8	1 263	2.61 2.61	0.108 0.108
ER	12.86 128.7	1 263	26.29 26.29	<0.001 <0.001	0.735 140.8	1 263	1.37 1.37	0.243 0.243
WDR	313.6 $1.55 \cdot 10^4$	1 263	5.33 5.33	0.022 0.022	28.22 $1.58 \cdot 10^4$	1 263	0.47 0.47	0.493 0.493
$W_{bf}$	18.07 $1.86 \cdot 10^4$	1 263	0.26 0.26	0.614 0.614	0.102 18.603	1 263	0.001 0.001	0.970 0.970
$MD_{bf}$	2.270 65.66	1 263	9.09 9.09	0.003 0.003	1.245 66.68	1 263	4.91 4.91	0.027 0.027

satisfactory for all the models that assumed the null hypothesis of equal variances ( $p > .05$ ).

#### 5. Conclusions

Ephemeral streams have extraordinary dynamics that are strongly conditioned by changes in climate, land cover and human impacts. Variability in dimensionless morphological ratios (DMR) can be used as an appropriate indicator of this dynamism at different scales, both temporally and spatially. It is commonly assumed that changes in the incision and width-to-depth ratios (WDR) often correspond to human actions. However, in some instances, the entrenchment ratio (ER) reflects a disconnection with the floodplain that predates human settlement, which should not be viewed as a channel adjustment process in the short term. This is true of the stream reach studied here, where the relationships between DMR and channel metrics revealed a lack of consistent, significant correlation with each other. Only the ER maintained a moderate relationship with the incision ratios ( $IR_{upp}$  and  $IR_{low}$ ), maximum bankfull depth ( $MD_{bf}$ ) and flood prone width ( $W_{fp}$ ). The flow data at bankfull stage also presented patterns of spatial variability different from those of the DMR, depending on the degree of sinuosity and position in the meander curve (entry or exit). Patterns of bed stability and minor morphological adjustments, associated with the lowest values of excess mean stream power ( $\omega/\omega_c$ ) and the mean stream power gradient ( $\partial\omega/\partial s$ ), were found in moderately incised cross sections exhibiting low or no entrenchment and moderate WDR along bend stretches (BS), and in highly incised and entrenched cross sections with moderate to high WDR along straight channel stretches (SS). The threshold of the stream power for stability in the study ephemeral channel differed from that suggested by other researchers for perennial gravel-bed streams. In particular, cross sections with a more stable bed ( $RBS < 1$ ) the minimum  $\omega$  required for bed degradation exceeded  $80 \text{ W m}^{-2}$ . Under conditions of greater flow competence ( $1 < RBS < 2$ ), this value ranged from  $33 \text{ W m}^{-2}$  in moderately incised stream stretches ( $1 < IR < 2$ ) to  $42 \text{ W m}^{-2}$  in highly incised ones ( $IR > 2$ ). These results seem to confirm the existence of current morphological adjustments (a slowdown of scour processes by increasing bed armoring and channel widening) different from those developed at an earlier stage that were responsible for deep incision and entrenchment. At a spatial scale, the relationships between the excess of energy at cell i

and the IR and the WDR at cells  $i$  and  $i + j$  revealed an increasing dispersion as the lag distance increased, especially in straight stretches composed of transitional areas from alluvium to rock substrate. The statistical ANOVA found more significant differences between SS and BS than between stretches from the inflection point to the meander bend apex (IP-MBA) and stretches from the meander bend apex to the inflection point (MBA-IP), and highlighted the importance of  $IR_{low}$ , ER and  $MD_{bf}$  as influential discriminant variables in both classes of stretch type. This study provides spatial variability patterns of bankfull hydraulic parameters that are not always consistent with DMR, showing that there has been a substantial change in the recent dynamics of the ephemeral stream analyzed here. Furthermore, it offers a useful approach to identify geomorphic reference sites and supplies the morphological information necessary for any ephemeral stream restoration plan.

## Notation

BFS	bedform stability index [—]
bgu	bed geomorphic unit
BS	bend channel stretch
$D_{50}$	median grain size
$D_{84}$	particle size corresponding to the 84% of the sample weight
$D_h$	hydraulic depth [m]
DMR	dimensionless morphological ratio
ER	entrenchment ratio [—]
$Fr$	Froude number [—]
$g$	acceleration of gravity [ $\text{m s}^{-2}$ ]
$i$	cell at $i$ cross-section
IP-MBA	stretches from the inflection point to the meander bend apex
IR	incision ratio [—]
$j$	cell lag at $j$ cross-section
$LW_{bgu\ (sc)}$	locational weight assigned to each bgu along a given stretch class (sc) [—]
MBA-IP	stretches from the meander bend apex to the inflection point
$MD_{bf}$	maximum bankfull depth [m]
$n_i\ (sc)$	number of cross-sections included in each stretch class (sc)
$Q_{bf}$	bankfull discharge [ $\text{m}^3/\text{s}$ ]
R	hydraulic radius [m]
RBS	relative bed stability index [—]
$r^2$	determination coefficient
$S_w$	water surface slope [m/m]
sc	stream stretch class
SI	sinuosity index
SS	straight channel stretch
$v_{rbgu}$	value assigned to each type of bed geomorphic unit (bgu), depending on its resistance to erosion [—]
$w_{bgu}$	width of each bgu in a channel cross-section [m]
$W_a$	bend apex width [m]
$W_i$	inflection point width [m]
$W_p$	width at the bankfull channel with maximum bend pool scour [m]
$W_a/W_i$	ratio of bend apex width to inflection point width [—]
$W_p/W_i$	ratio of width at the location of maximum bend pool scour to inflection point width [—]
$W_{bf}$	bankfull width [m]
$W_{fp}$	flood prone width [m]
WDR	width-to-depth ratio [—]
$\partial\omega/\partial s$	mean stream power gradient [ $\text{W m}^{-2}/\text{m}$ ]
$\varepsilon_{(i)}$	excess energy per unit bed area over $\omega_c$ at cell $i$ [ $\text{W m}^{-2}\ \text{J}$ ]
$\gamma$	specific weight of water ( $\text{N/m}^3$ )
$\Omega$	cross-sectional stream power [ $\text{W m}^{-1}$ ]
$\omega$	mean stream power [ $\text{W m}^{-2}$ ]
$\omega_c$	critical mean stream power [ $\text{W m}^{-2}$ ]
$\rho$	density of water [ $\text{kg m}^{-3}$ ]
$\rho_s$	density of sediment [ $\text{kg m}^{-3}$ ]

$v$	flow velocity
$v_{bf}$	bankfull flow velocity
$\tau$	shear stress ( $\text{N m}^{-2}$ )
$\tau_{bf}$	shear stress at bankfull flow ( $\text{N m}^{-2}$ )
$\tau_{c84}$	critical shear stress required to mobilize $D_{84}$ -size particles ( $\text{N m}^{-2}$ )
$\tau_c^*$	critical values of the dimensionless Shields parameter

## Declaration of competing interests

The authors declare that they have no known competing financial interests or personal relationships that could have appeared to influence the work reported in this paper.

## Acknowledgments

This work has been financed by ERDF/Spanish Ministry of Science, Innovation and Universities - State Research Agency/Project CGL2017-84625-C2-1-R (CCAMICEM); State Program for Research, Development and Innovation focused on the Challenges of Society. We also would like to extend our thanks to the Segura River Hydrographic Confederation Center (SHC), Government of Spain, for its collaboration.

## References

- Alfonso-Torreño, A., Gómez-Gutiérrez, A., Schnabel, S., Lavado Contador, J.F., de SanjoseBlasco, J.J., Sanchez Fernandez, M., 2019. SUAS, SIM-MVS photogrammetry and a topographic algorithm method to quantify the volume of sediments retained in check-dams. *Sci. Total Environ.* 678, 369–382.
- Biron, P.M., Choné, G., Buffin-Bélanger, T., Demers, S., Olsen, T., 2013. Improvement of streams hydro-geomorphological assessment using LiDAR DEMs. *Earth Surf. Process. Landf.* 38, 1808–1821.
- Bizzi, S., Lerner, D.N., 2015. The use of stream power as an indicator of channel sensitivity to erosion and deposition processes. *River Res. Appl.* 31, 16–27.
- Brierley, G.J., Fryirs, K.A., 2005. *Geomorphology and River Management: Applications of the River Styles Framework*. John Wiley & Sons, ChichesterUK.
- Brookes, A., 1987. River channel adjustments downstream from channelization works in England and Wales. *Earth Surf. Process. Landf.* 12, 337–351.
- Bull, W.B., 1997. Discontinuous ephemeral streams. *Geomorphology* 19, 227–276.
- Camenen, B., 2012. Discussion of “Understanding the influence of slope on the threshold of coarsegrainmotion: Revisiting critical stream power” by Parker, C., Clifford, N.J. and Thorne, C.R. (2011), *Geomorphology*, 126: 51–65. *Geomorphology* 139–140, 34–38.
- Camporeale, C., Perona, P., Ridolfi, L., 2006. Hydrological and geomorphological significance of riparian vegetation in drylands. In: D’Odorico, P., Porporato, A. (Eds.), *Dryland Ecohydrology*. Springer Verlag, Dordrecht, The Netherlands, pp. 161–179.
- Charlton, R., 2008. *Fundamentals of Fluvial Geomorphology*. Routledge, New York, pp. 4–7.
- Chen, S.A., Michaelides, K., Grieve, S.W.D., Singer, M.B., 2019. Aridity is expressed in river topography globally. *Nature* 573, 573–577.
- CHS, 2002. Proyecto de corrección hidrológica de las cuencas de la Cierva. Pliego y Los Roedos, Murcia, p. 408.
- Conesa García, C., García Lorenzo, R., 2007. Erosión y diques de retención en la Cuena Mediterránea. Efectividad hidrogeomorfológica de los diques de retención en cuencas torrenciales del Sureste Español. Fundación Instituto Euromediterráneo del Agua, Murcia, p. 669.
- Conesa-García, C., Pérez-Cutillas, P., García-Lorenzo, R., Gómez-Gutiérrez, A., Eekhout, J., Ibáñez, A., Ollero, A., Horacio, J., 2019. Mapping spatial patterns of dimensionless ratios along an ephemeral channel using SIM photogrammetry. *Geophys. Res. Abstr.* 21 EGU2019-7613-1, 2019 EGU, Vienna.
- Das, B.C., 2015. Modeling of most efficient channel form: a quantitative approach. *Model. Earth Syst. Environ.* 1, 15.
- Ezzat, R.Z., Oak, R.A., 2012. Application of Rosgen classification of rivers to an Indian river – a case study. *Int. J. Adv. Eng. Technol.* 3 (1), 367–370.
- Finnegan, N.J., Roe, G., Montgomery, D.R., Hallet, B., 2005. Controls on the channel width of rivers: implications for modeling fluvial incision of bedrock. *Geology* 33 (3), 229–232.
- Garzón, G., Alonso, A., 2002. Comparison of the flood response of a braided and a meandering river, conditioned by anthropogenic and climatic changes. In: Martini, I.P., Baker, V.R., Garzón, G. (Eds.), *Flood and Megaflood Processes and Deposits: Recent and Ancient Examples*. Blackwell Publishing Ltd., Oxford.
- Golly, A., Turowski, J.M., 2017. Deriving principal channel metrics from bank and long-profile geometry with the R package cmgo. *Earth Surf. Dyn.* 5, 557–570.
- Goodrich, D.C., Lane, L.J., Shillito, R.M., Miller, S.N., Syed, K.H., Woolhiser, D.A., 1997. Linearity of basin response as a function of scale in a semiarid watershed. *Water Resour. Res.* 33 (12), 2951–2965.
- Hamshaw, S.D., Engel, T., Rizzo, D.M., O’Neil-Dunne, J., Dewoolkar, M.M., 2019. Application of unmanned aircraft system (UAS) for monitoring bank erosion along river corridors. *Geomat. Nat. Haz. Risk* 10 (1), 1285–1305.

- Harvey, M.D., Watson, C.C., 1986. Fluvial processes and morphological thresholds in incised channel restoration. *Water Resour. Bull.* 3 (3), 359–368.
- Hooke, J.M., 2006. Human impacts on fluvial systems in the Mediterranean region. *Geomorphology* 79, 311–335.
- Juracek, K.E., Fitzpatrick, F.A., 2003. Limitations and implications of stream classification. *J. Am. Water Res. Assoc.* 39 (3), 659–670.
- Kasprak, A., Hough-Snee, N., Beechie, T., Bouwes, N., Brierley, G., Camp, R., 2016. The blurred line between form and process: a comparison of stream channel classification frameworks. *PLoS One* 11 (3), e0150293.
- Ken, M., Fritz, K.M., Johnson, B.R., Walters, D.M., 2008. Physical indicators of hydrologic permanence in forested headwater streams. *J. N. Am. Benthol. Soc.* 27 (3), 690–704.
- Krapesch, G., Habersack, H., 2011. Scale orientated analysis of river width changes due to extreme flood hazards. *Nat. Hazards Earth Syst. Sci.* 11 (8), 2137–2147.
- Lea, D.M., Legleiter, C.J., 2015. Mapping spatial patterns of stream power and channel change along a gravel-bed river in northern Yellowstone. *Geomorphology* 252, 66–79.
- Leopold, L.B., 1994. *A View of the River*. Harvard University Press, Cambridge, MA.
- Leopold, L.B., Wolman, M.G., Miller, J.P., 1964. *Fluvial Processes in Geomorphology*. Dover Publications, Inc., New York.
- Levick, L.R., Goodrich, D.C., Mariano Hernandez, M., Pima, J.F., Semmens, D.J., Stromberg, J., Truczek, M., Leidy, R.A., Sciani, M., Guertin, D.P., Kepner, W.G., 2008. The Ecological and Hydrological Significance of Ephemeral and Intermittent Streams in the Arid and Semi-Arid American Southwest. U.S. Environmental Protection Agency, Office of Research and Development, Washington, p. 101.
- Luebke, M.A., 2006. *Entrenched Stream Channels in the Blue Ridge Mountains*. The University of Georgia, Athens, Georgia, p. 84.
- Magilligan, F.J., 1992. Thresholds and the spatial variability of flood power during extreme floods. *Geomorphology* 5, 373–390.
- Martínez Salvador, A., Conesa García, C., García Lorenzo, R., Pérez Cutillas, P., 2015. Estimación de aportes sedimentarios a embalses de pequeñas cuencas mediterráneas mediante GeoWEPP. Ensayo en la cuenca vertiente del río Mula al embalse de la Cierva (cuenca del río Segura). *Limnetica* 34 (1), 41–56.
- Martin-Vide, J.P., 1997. *Ingeniería Fluvial*. Universitat Politècnica de Catalunya, Barcelona, PolítextArea d'EnginyeriaCivik. Edicions UPC, p. 209.
- Merritt, D.M., Wohl, E.E., 2003. Downstream hydraulic geometry and channel adjustment during a flood along an ephemeral, arid-region drainage. *Geomorphology* 52, 165–180.
- Mueller, J.R., 1968. An introduction to the hydraulic and topographic sinuosity indexes. *Ann. Assoc. Am. Geogr.* 58 (2), 371–385.
- Norman, L.M., Sankey, J.B., Dean, D., Caster, J., DeLong, S., DeLong, W., Pelletier, J., 2017. Quantifying geomorphic change at ephemeral stream restoration sites using a coupled-model approach. *Geomorphology* 283, 1–16.
- NRCS (Natural Resources Conservation Service), 2007a. Stream Restoration Design (National Engineering Handbook 654), Chapter 11: Rosgen Geomorphic Channel Design. United States Department of Agriculture, USDA, pp. 11–76.
- NRCS (Natural Resources Conservation Service), 2007b. Stream Restoration Design (National Engineering Handbook 654), Chapter 12: Channel Alignment and Variability Design. United States Department of Agriculture, USDA, pp. 12–31.
- Olsen, D.S., Whitaker, A.C., Potts, D.F., 1997. Assessing stream channel stability thresholds using flow competence estimates at bankfull stage. *J. Am. Water Resour. Assoc.* 33, 1197–1207.
- Ortega, J.A., Razola, L., Garzón, G., 2014. Recent human impacts and change in dynamics and morphology of ephemeral rivers. *Nat. Hazards Earth Syst. Sci.* 14 (3), 713–730.
- Parker, C., Clifford, N.F., Thorne, C.R., 2011. Understanding the influence of slope on the threshold of coarse grain motion: revisiting critical stream power. *Geomorphology* 126, 51–65.
- Reid, I., Frostick, L.E., 2011. Channel form, flows and sediments of endogenous ephemeral rivers in deserts. In: Thomas, D.S.G. (Ed.), *Arid Zone Geomorphology: Process, Form and Change in Drylands*, Third edition John Wiley & Sons, Chichester, pp. 301–332.
- Richards, K.S., 1982. *Rivers: Form and Process in Alluvial Channels*. Methuen, London, p. 361.
- Rickermann, D., Recking, A., 2011. Evaluation of flow resistance in gravel bed rivers through a large field data set. *Water Resour. Res.* 47, 1–23.
- Rodríguez Estrella, T., Navarro Hervás, F., 2001. Desprendimientos y vuelcos en laderas, desencadenados por sismicidad en la cuenca de Mula (Murcia). In: Manero, F. (Ed.), *Espacio natural y dinámicas territoriales. Libro homenaje al doctor D. Jesús García Fernández*. Universidad de Valladolid, pp. 171–182.
- Rosgen, D.L., 1996. *Applied River Morphology*. Wild-land Hydrology, Pagosa Springs, Colorado, USA.
- Rosgen, D.L., 1997. A geomorphological approach to restoration of incised rivers. In: Wang, S.S.Y., Langendoen, E.J., Shields, F.D. (Eds.), *Proceedings of the Conference on Management of Landscapes Disturbed by Channel Incision*. The University of Mississippi, Oxford.
- Schumm, S.A., 1960. The shape of alluvial channels in relation to sediment type. *US Geol. Surv. Prof. Pap.* 352B, 17–30.
- Segura-Beltrán, F., Sanchís-Ibor, C., 2013. Assessment of channel changes in a Mediterranean ephemeral stream since the early twentieth century. *The Rambla de Cervera, eastern Spain*. *Geomorphology* 201, 199–214.
- Shaw, J.R., Cooper, D.J., 2008. Linkages among watersheds, stream reaches, and riparian vegetation in dryland ephemeral stream networks. *J. Hydrol.* 350, 68–82.
- Simon, A., Castro, J., 2003. Measurement and analysis of alluvial channel form. In: Kondolf, G.M., Pieglay, H. (Eds.), *Tools in fluvial geomorphology*. Wiley, pp. 291–322.
- Simon, A.E., Darby, S., 1997. Process-form interactions in unstable sand bed river channels: a numerical modelling approach. *Geomorphology* 21, 85–106.
- Simon, A., Rinaldi, M., 2006. Disturbance, stream incision and channel evolution: the roles of excess transport capacity and boundary materials in controlling channel response. *Geomorphology* 79, 361–383.
- Stacey, M., Rutherford, I., 2007. Testing specific stream power thresholds of channel stability with GIS. *Proceedings of the 5th Australian Stream Management Conference. Australian rivers: making a difference*. Charles Sturt University, Thuringowa, New South Wales, pp. 384–389.
- Stewardson, M.J., 2005. Hydraulic geometry of stream reaches. *J. Hydrol.* 306, 97–111.
- Sutfin, N., Shaw, J., Wohl, E., Cooper, D.J., 2014. A geomorphic classification of ephemeral channels in a mountainous, arid region, southwestern Arizona, USA. *Geomorphology* 221, 164–175.
- Tamminga, A., Hugenholtz, C., Eaton, B., Lapointe, M., 2015. Hyperspatial remote sensing of channel reach morphology and hydraulic fish habitat using an unmanned aerial vehicle (UAV): a first assessment in the context of river research and management. *River Res. Appl.* 31 (3), 379–391.
- USACE (United States Army Corps of Engineers), 2002. *HEC-RAS: River Analysis System. Hydraulic Reference Manual, Version 5.0*. Hydrologic Engineering Center, Washington, D.C., p. 74.
- Walters, D.M., Leigh, D.S., Freeman, M.C., Freeman, B.J., Pringle, C.M., 2003. Geomorphology and fish assemblages in a piedmont river basin, USA. *Freshw. Biol.* 48, 1950–1970.
- Wampler, P.J., 2012. Rivers and streams – water and sediment in motion. *Nat. Educ. Knowl.* 3 (10), 18.
- Wharton, G., 1995. The channel-geometry method: guidelines and application. *Earth Surf. Process. Landf.* 20, 49–660.
- Wittenberg, L., Laronne, J.B., Newson, M.D., 2007. Bed clusters in humid perennial and Mediterranean ephemeral gravel-bed streams: the effect of clast size and bed material sorting. *J. Hydrol.* 334, 312–318.
- Zones, C.M., 2004. *Standard Methods for Identifying Bankfull Features and Channel Migration Zones*, Section 2. Washington State Department of Natural Resources, Washington.